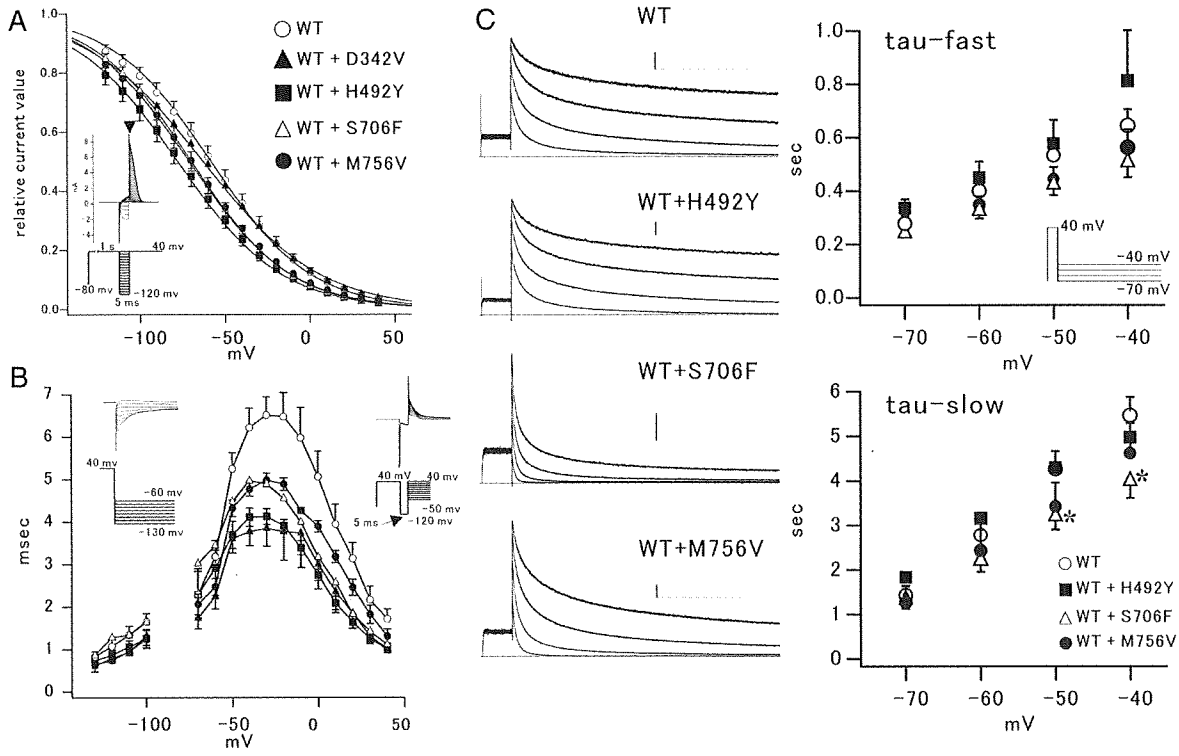

Figure 4. Multiple gating defects associated with KCNH2 mutations. A, Mutations associated with drug-induced arrhythmia caused a negative shift of inactivation gate of *KCNH2* channels. Steady-state channel availability as a function of membrane potential was measured by using a double-step method, as shown in the insets: the voltage-clamp protocol and original current traces from a representative cell expressing WT *KCNH2* channels. Open circles indicate the inactivation calculated from cells expressing cDNA with WT (2 μg), closed triangles, D342V/WT; closed squares, H492Y/WT; open triangles, S706F/WT; and closed circles, M756V/WT. All data were taken from 14 to 20 cells except for D342V/WT. B, To examine the inactivation time course, a conditioning pulse to +40 mV for 900 ms from a holding potential of −80 mV was followed by a hyperpolarizing pulse to −120 mV for 5 ms, and subsequent depolarizing test pulses between −50 and +40 mV in 10 mV steps were applied. In addition, a conditioning pulse to +40 mV for 750 ms was applied from a holding potential of −80 mV, followed by test pulses to various potentials between −130 and −60 mV in 10 mV increments. The inset illustrates the voltage protocol. Inactivation time constants were measured by fitting inactivating currents during test pulses at each potential with a single exponential function. C, The S706F/*KCNH2* mutant channel slightly accelerates deactivation time course. Left column, time course of deactivation for each channel. To examine the deactivation time course, a conditioning pulse to +40 mV for 1.6 seconds from a holding potential of −80 mV was followed by hyperpolarizing test pulses between −70 mV and −40 mV in 10-mV increments for 16 seconds (inset). Currents were not leak-subtracted. Each inset illustrates scale bars of 200-pA and 5-second times. Deactivation time constants (tau) were measured by fitting deactivating currents during test pulses at each potential with double exponentials. The slow components of tau for the S706F/WT channel were smaller than that of WT; *$P<0.05$.

availability to the hyperpolarizing direction compared with WT ($V_{1/2}$ of −58.3±4.7 mV for WT, $V_{1/2}$ of −61.4±6.5 mV for D342V/WT, −77.8±4.7 mV for H492Y/WT, −70.1±3.2 mV for S706F/WT, and −71.1±4.6 mV for M756V/WT, respectively). The time course to recovery from or the development of the inactivation (recovery from inactivation at hyperpolarized potentials and development of inactivation at >−70 mV) was analyzed by double or triple pulse protocols. The time course of inactivating kinetics could be fitted by a single-exponential function. Time constants thus calculated were significantly smaller than WT and mutant channels over a wide range of voltage (between −50 and +40 mV for D342V/WT and H492Y/WT; between −30 and +20 mV for S706F/WT; between −40 and 0 mV for M756V/WT, Figure 4B). These results demonstrate that drug-induced LQTS mutants have accelerated inactivation kinetics. Figure 4C shows representative families of current traces (left panel) and time constants (right panel) of deactivation in each channel. When the time course of deactivating kinetics was fitted by a double-exponential function, the S706F/WT channel slightly accelerated the deactivation process (Figure 4C).

Most of the drugs that induced LQTS in the study subjects have been known to block I_{Kr} in a concentration-dependent manner,[8,17,19–22] whereas I_{Kr} channel with *KCNH2* mutations may have different drug sensitivities compared with the WT channel. Figure 5 shows 3 sets of drug concentration-current inhibition relationships associated with *KCNH2* mutations with respect to erythromycin (5A), disopyramide (5B), and pirmenol (5C). In each case of drug-induced LQTS, an electrophysiological assay of current inhibition by the respective culprit drug was performed, for example, hydroxyzine,[17] erythromycin, disopyramide, and pirmenol. IC_{50}s were not significantly different between WT and the respective mutant channels, suggesting that a change in drug sensitivity was not involved in causing the drug-induced TdP in the study subjects.

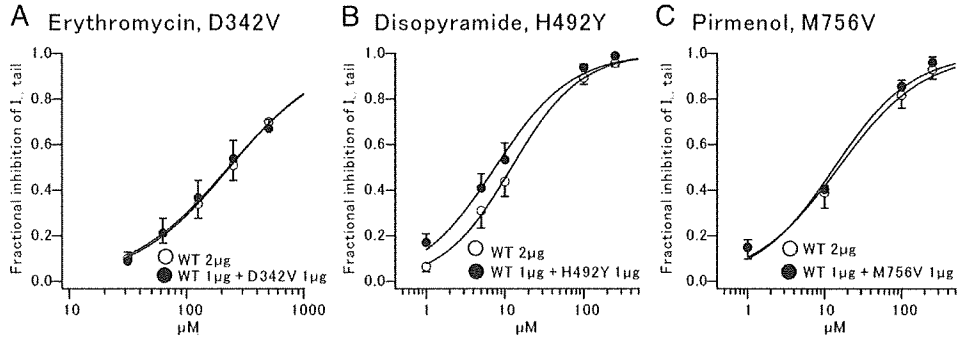

Figure 5. Both WT and mutant channels showed similar drug sensitivities to the culprit agents. A, Fractional blockade by micromolar erythromycin was recorded with regard to D342V/WT or WT as described in the methods and is plotted against the drug concentrations. B, Similarly, the relationship between the fractional block by disopyramide and its concentration are shown. C, The relationship between the fractional pirmenol block of M756V/WT or WT channels and its concentration. IC_{50}s for erythromycin, disopyramide, and pirmenol were 327 μmol/L (WT) and 248 μmol/L (D342V/WT), 13.9 μmol/L (WT) and 8.4 μmol/L (H492Y/WT), and 16.6 μmol/L (WT) and 13.4 μmol/L (M756V/WT), respectively (n=4 or 5 cells per condition).

Computer Simulation of Ventricular Action Potentials

To compare how the functional changes caused by mutants affect ventricular action potentials, a simulation study was conducted using the Luo-Rudy computer model that incorporated the Markov[16] or Hodgkin-Huxley[23] process gating for the mutant channels (Figure 6A). Table 2 shows parameters of simulation that have been changed to fit to experimental results. First, the I_{Kr} or I_{Ks} conductance was reduced to the level observed in the D342V/WT, A614V/WT, and R231C/WT channels. The deactivation time course for R231C/WT was also fitted by modifying a parameter. Second, the transition rate was changed accordingly from inactivation to open states (αi) and fitted with the experimental data seen in H492Y/WT and M756V/WT channels. Acceleration of inactivation induced by modifying the transition rate αi reproduced smaller amplitudes for I-V relationships and negative shift of steady-state inactivation curve (Figure 4A); these findings were compatible with the experimental results (Figure 3, A through C). Third, some parameters were altered to simulate the S706F/WT model, by reducing the I_{Kr} conductance, modifying αi, and increasing the transition rate from open to deactivation states. This was followed by change to parameters associated with the activation and deactivation rates for the R243H/WT model. Finally, not only was I_{Na} conductance decreased in the subjects, but the burst mode was also added to simulate the sustained current for the L1825P model.[24] The L1825P/WT channel was heterogeneously simulated to equally mix WT and L1825P models.

In the simulated M cells using the Luo-Rudy model, the order of increase in magnitude of action potential duration (APD) was A614V/WT>R231C/WT>D342V/WT>S706S/WT>R243H/WT=L1825P/WT >H492Y/WT>M756V/WT for dLQTS mutations (Figure 6B, middle panel). Typically, for cLQTS mutations, the simulated APD was longer than for WT or drug-induced models, whereas APDs in drug-induced models were intermediate between those in WT and those in cLQTS (clinical information for simulated cLQTS are presented in supplemental Table 1).

Finally, an effort was made to reproduce action potentials in the presence of I_{Kr}-blocking drugs (Figure 6C). Early afterdepolarizations appeared in all mutants where there were smaller reductions in the I_{Kr} conductance compared with the corresponding WT. Because drug sensitivities for WT and mutant channels were not different (Figure 5), the same inhibition rate was used in both the WT and mutant models and the I_{Kr} conductance was gradually reduced at the cycle length of 1200 ms. As shown in Figure 6C, typically, when the I_{Kr} conductance was theoretically decreased to 89% of the basal conductance for each channel, the D342V/WT model began to develop early afterdepolarizations, whereas the WT model produced only a 2.9% increase in APD.

Discussion

There were 3 major findings.[1] In 8 of 20 consecutive dLQTS subjects, 5 *KCNH2*, 2 *KCNQ1*, and 1 *SCN5A* heterozygous missense mutations were identified; there was a similar positive mutation rate with dLQTS compared with cLQTS.[2] Both *KCNQ1* and *KCNH2* mutants possessed loss of function effects on reconstituted I_{Ks}- or I_{Kr}-like channels.[3] The functional changes in mutant channels reconstituted by the computer simulation resulted in a mildly prolonged APD, suggesting that the dLQTS may partially have a genetic background, especially mild or latent long-QT syndrome–associated mutations.

Mutations in dLQTS

Potential torsadegenic drugs are used in the clinical setting and include antiarrhythmic drugs, antibiotics, antihistamines, psychiatric drugs, and cholinergic antagonists. These might induce TdP, which may lead to the sudden cardiac death of individuals whose QT intervals were within normal range before taking the drug. Several drugs such as cisapride and terfenadine have been withdrawn from the market because of these possible side effects.[25,26] The incidence of dLQTS is not high, and the drugs lead to TdP in only a small percentage of individuals, suggesting that there may be an underlying genetic background that predisposes these individuals to the risk.

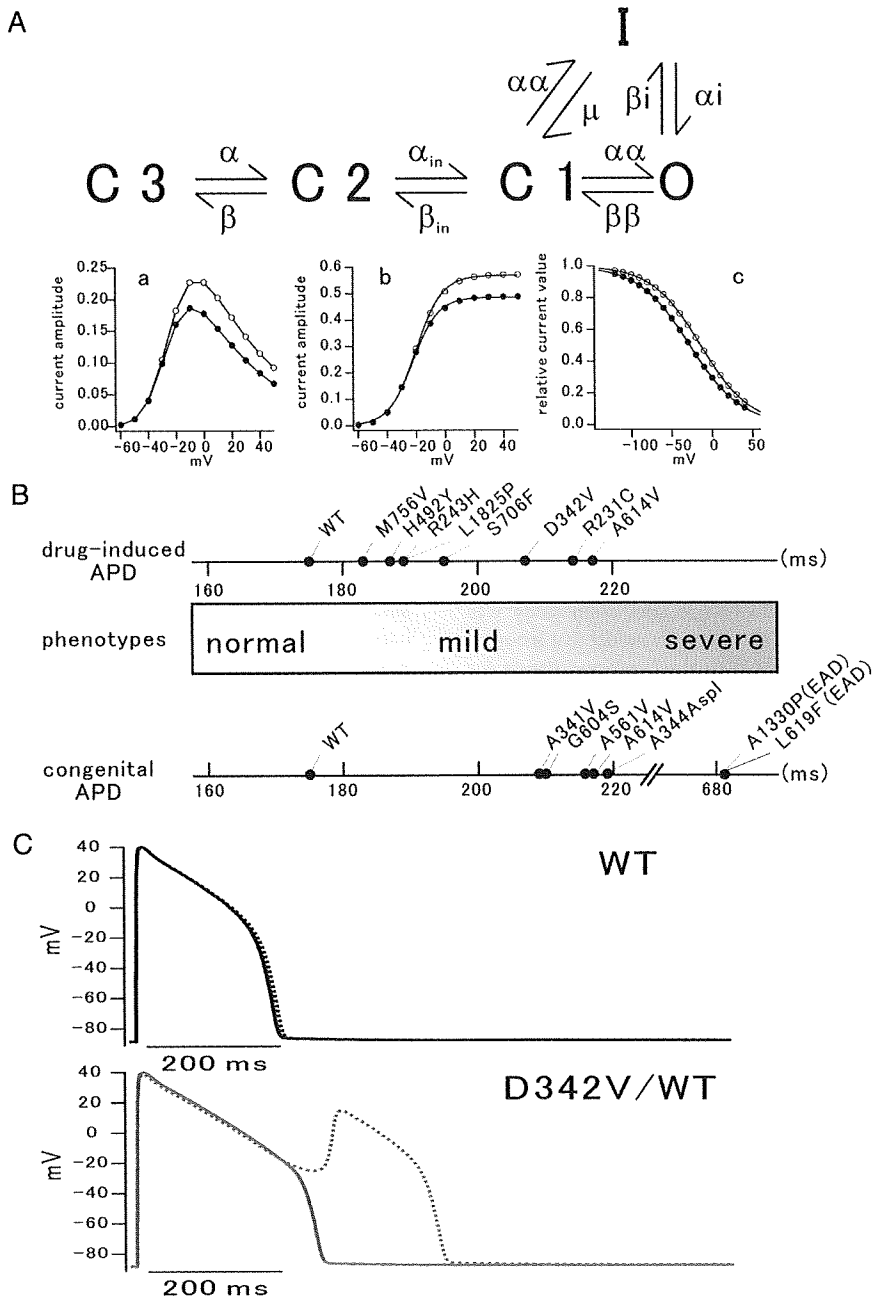

Figure 6. Simulation study of congenital and dLQTS-associated channels. A, Scheme showing a Markov model for I_{Kr} channels and simulation results for voltage-clamp protocols with a modified the transition rate αi; $\alpha i = 0.439 \times \exp(-0.02352 \times (V + 40))/K_{out}$. The 3 panels illustrate the result on the M756V/WT model, (a); the I-V relationship, (b); the I-V relationship for amplitudes of peak tail currents and (c); the steady-state inactivation curves. Open circles, WT; filled circles, mutant. B, Simulation study of action potential durations (APD). The parameters used for simulation were changed and matched the experimental results for voltage-clamp protocols. Myocardium models were stimulated at the cycle length of 600 ms for 5 minutes. C, Simulated APDs with I_{Kr}-blocking effects. When I_{Kr} conductance was decreased to 11% in each of the models, the D342V model showed early afterdepolarization, whereas the WT model had only slight prolonged APD. Bold lines, controls; dotted lines, models with I_{Kr}-blocking effects.

In the medical literature, 13 *KCNQ1* or *KCNH2* mutations (13 of 15 mutations, 87%) associated with dLQTS, including 6 of the mutations identified in this present study, have been located in nonpore regions (Figure 1B). Mutations in nontransmembrane regions have been shown to cause either mild long-QT syndrome or benign clinical phenotypes.[27] Mutation sites may influence the clinical and basic electrophysiological characteristics of patients with dLQTS. It is of interest that

Table 2. Parameters of Simulation Data in LQTS

Phenotype	Gene	Mutant	WT Basal Parameters	Mutant Changed Parameters
dLQTS	*KCNQ1*	R231C	gks=0.202*(1+0.6/(1+pow((0.000038/cai), 1.4)))	gks=0.103*(1+0.6/(1+pow((0.000038/cai), 1.4)))
			tauxs1=1/(0.0000719*(v+30)/(1−exp(−0.148...	tauxs1=1.1/(0.0000719*(v+30)/(1−exp(−0.148...
dLQTS	*KCNQ1*	R243H	xs1ss=1/(1+exp(− (v−1.5)/16.7))	xs1ss=1/(1+exp(− (v−11.5)/16.7))
			tauxs1=1/(0.0000719*(v+30)/(1−exp(−0.148...	tauxs1=0.9/(0.0000719*(v+30)/(1−exp(−0.148...
dLQTS	*KCNH2*	D342V	gherg=0.0135*pow(Kout, 0.59)	gherg=0.0043*pow(Kout, 0.59)
dLQTS	*KCNH2*	H492Y	αi=0.439*exp(−0.02352*(v+25))*4.5/Kout	αi=0.439*exp(−0.02352*(v+47))*4.5/Kout
dLQTS	*KCNH2*	S706F	gherg=0.0135*pow(Kout, 0.59)	gherg=0.0096*pow(Kout, 0.59)
			αi=0.439*exp(−0.02352*(v+25))*4.5/Kout	αi=0.439*exp(−0.02352*(v+39))*4.5/Kout
			bβ=2.9375e-3*exp(−0.02158*v)	bβ=5.875e-3*exp(−0.02158*v)
dLQTS	*KCNH2*	M756V	αi=0.439*exp(−0.02352*(v+25))*4.5/Kout	αi=0.439*exp(−0.02352*(v+40))*4.5/Kout
dLQTS	*KCNH2*	A614V	gherg=0.0135*pow(Kout, 0.59)	gherg=0.0024*pow(Kout, 0.59)
dLQTS	*SCN5A*	L1825P	G_{Na}=16	G_{Na}=1.76
			No burst mode	α6=5*e-6
			No burst mode	β6=3.34*e-4
cLQTS	*KCNQ1*	A341V	gks=0.202*(1+0.6/(1+pow((0.000038/cai), 1.4)))	gks=0.101*(1+0.6/(1+pow((0.000038/cai), 1.4)))
cLQTS	*KCNQ1*	A344AspI	gks=0.202*(1+0.6/(1+pow((0.000038/cai), 1.4)))	gks=0.087*(1+0.6/(1+pow((0.000038/cai), 1.4)))
cLQTS	*KCNH2*	A561V	gherg=0.0135*pow(Kout, 0.59)	gherg=0.0023*pow(Kout, 0.59)
			aα=65.5e-3*exp(0.05547153*(v−36))	aα=65.5e-3*exp(0.05547153*(v-16))
cLQTS	*KCNH2*	G604S	gherg=0.0135*pow(Kout, 0.59)	gherg=0.0040*pow(Kout, 0.59)
			αi=0.439*exp(−0.02352*(v+25))*4.5/Kout	αi=0.439*exp(−0.02352*(v+35))*4.5/Kout
cLQTS	*KCNH2*	A614V	gherg=0.0135*pow(Kout, 0.59)	gherg=0.0024*pow(Kout, 0.59)
cLQTS	*SCN5A*	L619F	G_{Na}=16	G_{Na}=6.24
			No burst mode	α6=10*e-6
			No burst mode	β6=3*e-4
cLQTS	*SCN5A*	L1330P	G_{Na}=16	G_{Na}=6.24
			No burst mode	α6=10*e-6
			No burst mode	β6=3*e-4

the functional assay of our 7 mutations resulted in various levels of loss of function, but most of them showed no dominant negative suppression, which is usually observed in the classic cLQTS. Clinical characteristics during the drug intake were not significantly distinct from those of cLQTS, which shares a similar genetic background with the dLQTS. Several polymorphisms have been shown to be associated with dLQTS.[4,28] Abbott et al[4] identified a polymorphism (T8A) of the *KCNE2* gene encoding MiRP, a β-subunit for the I_{Kr} channel, which is present in 1.6% of the population and is associated with TdP induced by quinidine or sulfamethoxazole/trimethoprim administration. Splawski et al[28] also found a heterozygous polymorphism involving substitution of serine with tyrosine (S1102Y) in the sodium channel gene *SCN5A* among blacks that increased the risk for drug-induced TdP. The polymorphism was present in 57% of 23 patients with proarrhythmic episodes but in only 13% of control subjects. These findings suggested that common genetic variations may increase the risk for development of drug-related arrhythmias.

Roden et al[29] reported that cisapride could rescue trafficking of L1825P channel with a potentially sustained current and revealed a new mechanism of dLQTS with the Luo-Rudy model. However, in the genotyped subjects in the present study, dLQTS mainly resulted from the I_{Kr}-blocking effect of culprit drugs in the presence of latent genetic backgrounds. Cardiac repolarization reserve may protect subjects against the drug-induced QT prolongation by I_{Kr}-blocking drugs.[30,31] In the presence of latent genetic backgrounds, however, reduction in the repolarization reserve unveils the presence of so-called "concealed" long-QT syndrome when drugs with I_{Kr}-blocking effects are administered. The presence of borderline prolongation of the QT interval, together with personal information such as unexplained previous syncope and family history of premature sudden death, may help to prevent drug-induced arrhythmia even if a subject's Schwartz score is low, because they could have a potential risk of TdP. Special attention should be paid to family members of the index subject with drug-induced QT prolongation because ≈30% of family members were found to have a predisposing genetic background in the present study. Indeed, they may have inherited the risk for being susceptible to dLQTS.

Limitations of the Study

This study has some limitations. Bacause of the small cohort of dLQTS subjects, this study was not powered to quantify the overall prevalence of ion channel mutations in the group of subjects with drug-induced TdP; there was also a possible

selection bias in the population. As for the causative agents, we were unable to test the action of amphetamine and methamphetamine because it was impossible to obtain these illegal drugs for clinical study. However, a previous report has shown that 3,4-methylenedioxy methamphetamine (ecstasy, NMDA) prolongs the APD of hippocampal neurons by blocking the conductance of a resting K^+ channel.[32] It is quite possible that these drugs also suppressed cardiac K^+ currents and induced QT prolongation and TdP in 1 subject in our study, based on her medical records. Regarding protein trafficking, 2 mutations in this study, A614V in *KCNH2*[17] and L1825P in *SCN5A*,[29] had been reported to be trafficking-deficient mutations. Though protein trafficking of other mutants remains unclear, especially R243H in *KCNQ1*, and H492Y, S706F, and M756V in *KCNH2*, would be not trafficking-deficient because, under heterozygous conditions, these mutants showed adequate current density compared with WT. In the simulation study, the parameter settings could mimic mutant channels. In addition, the setting of the parameters might have innumerable patterns, and it therefore remains possible that other combinations of patterns could also simulate mutant channels.

Acknowledgments

We thank Arisa Ikeda for excellent technical assistance.

Sources of Funding

This work was supported by the Grant-in-Aid for Scientific Research from the Japan Society for the Promotion of Science and the Biosimulation and Health Sciences Research Grant (H18-Research on human Genome-002) from the Ministry of Health, Labor, and Welfare of Japan (M.H.) and a Grant-in-Aid for Young Scientists from the Ministry of Education, Culture and Technology of Japan (H.I.).

Disclosures

None

References

1. Schwartz PJ, Periti M, Malliani A. The long QT syndrome. *Am Heart J*. 1975;89:378–390.
2. Moss AJ, Schwartz PJ, Crampton RS, Tzivoni D, Locati EH, MacCluer J, Hall WJ, Weitkamp L, Vincent GM, Garson A Jr. The long-QT syndrome: prospective longitudinal study of 328 families. *Circulation*. 1991;84:1136–1144.
3. Haverkamp W, Breithardt G, Camm AJ, Janse MJ, Rosen MR, Antzelevitch C, Escande D, Franz M, Malik M, Moss A, Shah R. The potential for QT prolongation and proarrhythmia by non-antiarrhythmic drugs: clinical and regulatory implications: report on a policy conference of the European Society of Cardiology. *Eur Heart J*. 2000;21:1216–1231.
4. Sesti F, Abbott GW, Wei J, Murray KT, Saksena S, Schwartz PJ, Priori SG, Roden DM, George AL Jr, Goldstein SA. A common polymorphism associated with antibiotic-induced cardiac arrhythmia. *Proc Natl Acad Sci U S A*. 2000;97:10613–10618.
5. Makita N, Horie M, Nakamura T, Ai T, Sasaki K, Yokoi H, Sakurai M, Sakuma I, Otani H, Sawa H, Kitabatake A. Drug-induced long-QT syndrome associated with a subclinical SCN5A mutation. *Circulation*. 2002;106:1269–1274.
6. Napolitano C, Schwartz PJ, Brown AM, Ronchetti E, Bianchi L, Pinnavaia A, Acquaro G, Priori SG. Evidence of a cardiac ion channel mutation underlying drug-induced QT prolongation and life-threatening arrhythmias. *J Cadiovasc Electrophysiol*. 2000;11:691–696.
7. Yang P, Kanki H, Drolet B, Yang T, Wei J, Viswanathan PC, Hohnloser SH, Shimizu W, Schwartz PJ, Stanton M, Murray KT, Norris K, George AL, Roden DM. Allelic variants in long-QT disease genes in patients with drug-associated torsades de pointes. *Circulation*. 2002;105:1943–1948.
8. Hayashi K, Shimizu M, Ino H, Yamaguchi M, Terai H, Hoshi H, Higashida H, Terashima N, Uno Y, Kanaya H, Mabuchi H. Probucol aggravates long QT syndrome associated with a novel missense mutation M124T in the N-terminus of HERG. *Clin Sci (Lond)*. 2004;107:175–182.
9. Bellocq C, Wilders R, Schott JJ, Louérat-Oriou B, Boisseau P, Le Marec H, Escande D, Baró I. A common antitussive drug, clobutinol, precipitates the long QT syndrome. *Mol Pharmacol*. 2004;66:1093–1102.
10. Lehtonen A, Fodstad H, Laitinen-Forsblom P, Toivonen L, Kontula K, Swan H. Further evidence of inherited long QT syndrome gene mutations in antiarrhythmic drug-induced torsades de pointes. *Heart Rhythm*. 2007;4:603–607.
11. Haverkamp W, Shenasa M, Borggrefe M, Breithardt G. *Cardiac Electrophysiology*. 4th ed. Philadelphia: Saunders; 1999:886–899.
12. Bazett HC. An analysis of the time relations of electrocardiograms. *Heart*. 1920;7:353–370.
13. Schwartz PJ, Moss AJ, Vincent GM, Crampton RS. Diagnostic criteria for the long QT syndrome: an update. *Circulation*. 1993;88:782–784.
14. Ohno S, Zankov DP, Yoshida H, Tsuji K, Makiyama T, Itoh H, Akao M, Hancox JC, Kita T, Horie M. N- and C-terminal KCNE1 mutations cause distinct phenotypes of long QT syndrome. *Heart Rhythm*. 2007;4:332–340.
15. Splawski I, Shen J, Timothy KW, Vincent GM, Lehmann MH, Keating MT. Genomic structure of three long QT syndrome genes: KVLQT1, HERG, and KCNE1. *Genomics*. 1998;51:86–97.
16. Clancy CE, Rudy Y. Cellular consequences of HERG mutations in the long QT syndrome: precursors to sudden cardiac death. *Cardiovasc Res*. 2001;50:301–313.
17. Sakaguchi T, Itoh H, Ding WG, Tsuji K, Nagaoka I, Oka Y, Ashihara T, Ito M, Yumoto Y, Kubota T, Zenda N, Higashi Y, Takeyama Y, Matsuura H, Horie M. Hydroxyzine, an H_1 receptor antagonist of first generation, inhibits reconstituted I_{Kr} currents. *J Pharmacol Sci*. 2008;108:462–471.
18. Nakajima T, Furukawa T, Tanaka T, Katayama Y, Nagai R, Nakamurea Y, Hiraoka M. Novel mechanism of HERG current suppression in LQT2: shift in voltage dependence of HERG inactivation. *Circ Res*. 1998;83:415–422.
19. Daleau P, Lessard E, Groleau MF, Turgeon J. Erythromycin blocks the rapid component of the delayed rectifier potassium current and lengthens repolarization of guinea pig ventricular myocytes. *Circulation*. 1995;91:3010–3016.
20. Paul AA, Witchel HJ, Hancox JC. Inhibition of HERG potassium channel current by the class Ia antiarrhythmic agent disopyramide. *Biochem Biophys Res Commun*. 2001;280:1243–1250.
21. Yoshida H, Horie M, Otani H, Takano H, Tsuji K, Kubota T, Fukunami M, Sasayama S. Characterization of a novel missense mutation in the pore of HERG in a patient with long QT syndrome. *J Cardiovasc Electrophysiol*. 1999;10:1262–1270.
22. Walker BD, Singleton CB, Bursill JA, Wyse KR, Valenzuela SM, Qiu MR, Breit SN, Campbell TJ. Inhibition of the human ether-a-go-go-related gene (HERG) potassium channel by cisapride: affinity for open and inactivated states. *Br J Pharmacol*. 1999;128:444–450.
23. Hodgkin AL, Huxley AF. A quantitative description of membrane current and its application to conduction and excitation in nerve. *J Physiol*. 1952;117:500–544.
24. Clancy CE, Rudy Y. Na+ channel mutation that causes both Brugada and long-QT syndrome phenotypes: a simulation study of mechanism. *Circulation*. 2002;105:1208–1213.
25. Wysowski DK, Bacsanyi J. Cisapride and fatal arrhythmia. *N Engl J Med*. 1996;335:290–291.
26. Monahan BP, Ferguson CL, Killeavy ES, Lloyd BK, Troy J, Cantilena LR Jr. Torsades de pointes occurring in association with terfenadine use. *JAMA*. 1990;264:2788–2790.
27. Donger C, Denjoy I, Berthet M, Neyroud N, Cruaud C, Bennaceur M, Chivoret G, Schwartz K, Coumel P, Guicheney P. KVLQT1 C-terminal missense mutation causes a forme fruste long-QT syndrome. *Circulation*. 1997;96:2778–2781.
28. Splawski I, Timothy KW, Tateyama M, Clancy CE, Malhotra A, Beggs AH, Cappuccio FP, Sagnella GA, Kass RS, Keating MT. Variants of

SCN5A sodium channel implicated in risk of cardiac arrhythmia. *Science*. 2002;297:1333–1336.
29. Liu K, Yang T, Viswanathan PC, Roden DM. New mechanism contributing to drug-induced arrhythmia: rescue of a misprocessed LQT3 mutant. *Circulation*. 2005;112:3239–3246.
30. Jost N, Virág L, Bitay M, Takács J, Lengyel C, Biliczki P, Nagy Z, Bogáts G, Lathrop DA, Papp JG, Varró A. Restricting excessive cardiac action potential and QT prolongation: a vital role for IKs in human ventricular muscle. *Circulation*. 2005;112:1392–1399.
31. Roden DM, Yang T. Protecting the heart against arrhythmias: potassium current physiology and repolarization reserve. *Circulation*. 2005;112:1376–1378.
32. Premkumar L, Ahern G. Blockade of a resting potassium channel and modulation of synaptic transmission by ecstasy in the hippocampus. *J Pharmacol Exp Ther*. 1995;274:718–722.

CLINICAL PERSPECTIVE

Drug-induced long-QT syndrome (dLQTS) is a disease associated with the appearance of a prolonged QT interval and torsades de pointes after taking a culprit drug or drugs; the QT interval usually returns to within normal range after a washout period of these drugs. The clinical phenotype of dLQTS that appears during administration of these drugs resembles that of congenital long-QT syndrome (cLQTS), and "latent" genetic factors may underlie the susceptibility of a subject to drug-induced serious adverse reactions, such as a long QT interval and torsades de pointes. In the analysis of cLQTS-associated genes encoding cardiac ion channel-composing proteins, this study revealed that dLQTS had a similar positive mutation rate compared with cLQTS. When reconstituted in Chinese hamster ovary cells, *KCNQ1* and *KCNH2* mutant channels showed complex gating defects without dominant negative effects or a relatively mild decreased current density. With the Luo-Rudy simulation model of action potentials, action potential durations of most mutant channels were between those of wild-type and cLQTS. In conclusion, although the dLQTS subjects had genetic backgrounds that were similar to cLQTS subjects, the functional changes associated with these mutations identified in dLQTS were different from those in cLQTS. Thus, we believe that dLQTS can be regarded as a latent form of long-QT syndrome. When I_{Kr}-blocking agents produce excessive QT prolongation, the underlying genetic background of the dLQTS subject should be taken into consideration, as would be the case with cLQTS.

RESEARCH ARTICLE

Human Mutation

OFFICIAL JOURNAL
HGVS
HUMAN GENOME VARIATION SOCIETY
www.hgvs.org

Novel KCNE3 Mutation Reduces Repolarizing Potassium Current and Associated With Long QT Syndrome

Seiko Ohno,[1] Futoshi Toyoda,[2] Dimitar P Zankov,[2,3] Hidetada Yoshida,[1] Takeru Makiyama,[1] Keiko Tsuji,[3] Toshihiro Honda,[4] Kazuhiko Obayashi,[5] Hisao Ueyama,[6] Wataru Shimizu,[7] Yoshihiro Miyamoto,[8] Shiro Kamakura,[7] Hiroshi Matsuura,[2] Toru Kita,[1] and Minoru Horie[3]*

[1]*Department of Cardiovascular Medicine, Kyoto University Graduate School of Medicine, Kyoto, Japan*

[2]*Department of Physiology, Shiga University of Medical Science, Shiga, Japan*

[3]*Department of Cardiovascular and Respiratory Medicine, Shiga University of Medical Science, Shiga, Japan*

[4]*Cardiovascular Center, Saiseikai Kumamoto Hospital, Kumamoto, Japan*

[5]*Obayashi Clinic, Kyoto, Japan*

[6]*Department of Molecular Medical Biochemistry, Shiga University of Medical Science, Shiga, Japan*

[7]*Division of Cardiology, Department of Internal Medicine, National Cardiovascular Center, Osaka, Japan*

[8]*Laboratory of Molecular Genetics, National Cardiovascular Center, Osaka, Japan*

Communicated by Claude Férec

Received 25 January 2008; accepted revised manuscript 5 May 2008.
Published online 20 March 2009 in Wiley InterScience (www.interscience.wiley.com). DOI 10.1002/humu.20834

ABSTRACT: Long QT syndrome (LQTS) is an inherited disease involving mutations in the genes encoding a number of cardiac ion channels and a membrane adaptor protein. Among the genes that are responsible for LQTS, *KCNE1* and *KCNE2* are members of the *KCNE* family of genes, and function as ancillary subunits of Kv channels. The third *KCNE* gene, *KCNE3*, is expressed in cardiac myocytes and interacts with *KCNQ1* to change the channel properties. However, *KCNE3* has never been linked to LQTS. To investigate the association between *KCNE3* and LQTS, we conducted a genetic screening of *KCNE3* mutations and single nucleotide polymorphisms (SNPs) in 485 Japanese LQTS probands using DHPLC-WAVE system and direct sequencing. Consequently, we identified two *KCNE3* missense mutations, located in the N- and C-terminal domains. The functional effects of these mutations were examined by heterologous expression systems using CHO cells stably expressing KCNQ1. One mutation, p.R99λH was identified in a 76-year-old woman who suffered torsades de pointes (TdP) after administration of disopyramide. Another mutation, p.T4A was identified in a 16-year-old boy and 67-year-old woman. Although the boy carried another *KCNH2* mutation, he was asymptomatic. On the other hand, the woman suffered from hypokalemia-induced TdP. In a series of electrophysiological analyses, the KCNQ1(Q1) +KCNE3(E3)-R99λH channel significantly reduced outward current compared to Q1+E3-WT, though the current density of the Q1+E3-T4A channel displayed no statistical significance. This is the first report of *KCNE3* mutations associated with LQTS. Screening for variants in the *KCNE3* gene is of clinical importance for LQTS patients.
Hum Mutat 30, 557–563, 2009. © 2009 Wiley-Liss, Inc.

KEY WORDS: long QT syndrome; LQTS; *KCNE3*; ion channel; molecular screening; electrophysiology

Introduction

Long QT syndrome (LQTS) is an inherited disease characterized by a prolonged QT interval and a high risk of sudden cardiac death due to peculiar ventricular tachycardia known as torsades de pointes (TdP) [Moss and Kass, 2005]. Most of the LQTS-causing genes encode ion channels, with particular regard to potassium (K) channels. Among them, *KCNE1* (E1) and *KCNE2* (E2) are members of the *KCNE* family (E1 through *KCNE5*) encoding a single-transmembrane-domain proteins. They are called MinK-related peptides (MiRPs) that function as ancillary subunits of Kv channels. In 1999, the third *KCNE* gene, *KCNE3* (ONIM *604433) (E3), was cloned by homology to E1 [Abbott et al., 1999]. In the functional analysis on the KCNQ1 (Q1) +E3 channel, E3 was shown to markedly change Q1 channel properties to yield those activating nearly instantaneously and linearly on voltage [Schroeder et al., 2000].

The expression of E3 in heart was examined and confirmed by northern blot analysis [Schroeder et al., 2000], real-time quantitative RT-PCR [Bendahhou et al., 2005; Lundquist et al., 2005, 2006] and in situ hybridization [Lundquist et al., 2005]. E3 was expressed in all regions of the human heart including left and right ventricles [Lundquist et al., 2005]. The expression level of E3 was larger than that of E2 in every region of the human heart, although smaller than that of E1 [Bendahhou et al., 2005; Lundquist et al., 2005, 2006]. Recently, E3 was reported to

S.O. and F.T. contributed equally to this work.

*Correspondence to: Minoru Horie, M.D., Ph.D., Department of Cardiovascular and Respiratory Medicine, Shiga University of Medical Science, Seta Tsukinowa-cho, Otsu, Shiga, Japan 520-2192. E-mail: horie@belle.shiga-med.ac.jp

Contract grant sponsor: Japan Society for the Promotion of Science; Contract grant sponsor: Ministry of Health, Labour and Welfare, Japan; Grant number: H18-Research on Human Genome-002.

establish a complex with Q1 along with E1 [Morin and Kobertz, 2007]. The Q1+E1+E3 complex generated the current with the combined properties of homomeric Q1+E1 and Q1+E3 complexes, as we previously reported the properties of Q1+E1+E2 complexes [Toyoda et al., 2006]. Taken together, the dysfunction of the Q1+E3 channel may reduce repolarizing K currents in the myocardium, which thereby prolongs the QT interval, although Q1–E3 channels have not yet been demonstrated in the heart.

Abbott et al. [2001] demonstrated a missense mutation of E3 (p.R83λH) in the patients of periodic paralysis. The reduced current densities of the E3-R83λH plus Kv3.4 complex channel in the skeletal muscle caused periodic paralysis, though the authors did not mention cardiac symptoms. More recently, Lundby et al. [2008] identified an E3 mutation (p.V17λM) from an early-onset lone atrial fibrillation (AF) patients. They performed functional analysis of E3-V17λM in coexpression with five kinds of potassium channels. As a result, they revealed increased activity of KV4.3+E3-V17λM and KCNH2+E3-V17λM channels.

During the genetic screening on 485 Japanese LQTS probands, we identified two novel E3 mutations and one reported single nucleotide polymorphism (SNP) (rs34604640:C>G; p.P39R). The mutations were p.T4A in the N-terminal and p.R99λH in the C-terminal. In the present study, we describe the clinical phenotypes of E3-related LQTS patients and the electrophysiological effects caused by these E3 mutations, and assess the probability of E3 as a candidate gene for LQTS.

Materials and Methods

Subjects

Study patients are comprised of 485 congenital and acquired LQTS probands showing prolongation of the QT interval (QTc≥460 ms) or documented TdP from 485 unrelated families. They were referred consecutively to either of our laboratories for genetic evaluation. All subjects submitted written informed consent in accordance with the guidelines approved by each institutional review board. Each underwent detailed clinical and cardiovascular examinations, and were then characterized on the basis of the QT interval in lead V_5 corrected for heart rate (QTc) according to Bazett's formula and the presence of cardiac symptoms.

Genotyping

Genomic DNA was isolated from venous blood lymphocytes as previously described [Ohno et al., 2007]. Through PCR, denaturing high-performance liquid chromatography (DHPLC), and direct DNA sequencing, we performed a comprehensive open reading frame/splice-site mutational analysis of known LQTS genes (*KCNQ1*, *KCNH2*, *SCN5A*, *KCNE1*, and *KCNE2*) using previously described primers [Ohno et al., 2007]. We did not conduct mutational analysis of *ANKB*, *KCNJ2*, *CACNA1C*, *CAV3*, and *SCN4B*. The *KCNE3* coding region was amplified with a primer pair; forward primer; 5′-CTGAGCTTCTACCGAGTCTT-3′ and reverse primer; 5′-TGCAGTCCACAGCAGAGTTC-3′. The size of the PCR product was 435 base pairs. DHPLC analysis of *KCNE3* was performed at three different temperatures; 59.0, 61.2, and 63.5°C. The cDNA sequence was based on GenBank reference sequence NM_005472.4, and the numbering reflects cDNA numbering with +1 corresponding to the A of the ATG translation initiation codon in the reference sequence, according to journal guidelines. The initiation codon is codon 1.

Plasmid Construction

cDNA for human *KCNE3* (NM_005472.4) was cloned into a PCR3.1 plasmid. Variant amino acid residues were constructed using a Quick Change® II XL Site-Directed Mutagenesis Kit (Stratagene, La Jolla, CA), according to the manufacturer's instructions. Nucleotide sequence analysis was performed on each variant construct prior to the expression study.

Construction of a CHO Cell Line Stably Expressing Human KCNQ1

Flp-In CHO cells containing a single integrated Flp recombinase target (FRT) site at a transcriptionally active locus (Invitrogen, Carlsbad, CA) were used for the generation of a stable KCNQ1 cell line. The full-length cDNA fragment of human *KCNQ1* (GenBank AF000571.1) in a pCI vector (a kind gift from Dr. J. Barhanin, Institut de Pharmacologie Moléculaire et Cellulaire, CNRS, Valbonne, France) was subcloned into a pcDNA5/FRT vector (Invitrogen). This construct was cotransfected into Flp-In CHO cells with pOG44, a Flp-recombinase expression vector (Invitrogen), resulting in the targeting interaction of the expression vector. Stable cell clones were selected in hygromycin B (500 μg/ml; Invitrogen), and the expression of KCNQ1 was tested by the whole-cell patch-clamp recording method. One cell line exhibited uniform and homogenous expression of KCNQ1 currents and was used for experiments.

Cell Culture and Transient Transfection

The stable KCNQ1-CHO cell line was maintained in Ham's F-12 medium supplemented with 10% fetal calf serum and 500 &mug/ml hygromycin B in a humidified incubator gassed with 5% CO_2 and 95% air at 37°C. Before transfection, cells were seeded onto 35-mm plastic culture dishes with seven to eight glass coverslips (5λmm × 3λmm) and incubated for 24 to 48λhr. Transient transfection was performed using Lipofectamine (Invitrogen). The amounts of each cDNA used for transfection were (mug/dish): 1.0 *KCNE3*, and 0.5 green fluorescent protein (GFP). At 48 to 72λhr after transfection, only GFP-positive cells were selected for the patch-clamp study.

Patch-Clamp Recordings and Data Analysis

Whole-cell membrane currents were recorded with an EPC-8 patch-clamp amplifier (HEKA, Lambrecht, Germany). A coverslip with adherent CHO cells was placed on the glass bottom of a recording chamber (0.5λml in volume) mounted on the stage of Nikon Diaphot inverted microscope (Tokyo, Japan). Patch pipettes were prepared from glass capillary tube (Narishige, Tokyo, Japan) by means of a Sutter P-97 micropipette puller (Novato, CA), and the tips were then fire-polished with a microforge. Pipette resistance ranged from 2 to 4 Mω when filled with internal solution. Current recordings were conducted at 34±1°C. Voltage-clamp protocols and data acquisition were controlled by PatchMaster software (version 2.03, HEKA) via an LIH-1600 AD/DA interface (HEKA). Cell membrane capacitance (Cm) was measured in every cell by fitting a single exponential function to capacitive transients elicited by 20 ms voltage-clamp steps from a holding potential of −80 mV.

External Tyrode solution contained (mM): 140 NaCl, 0.33 NaH_2PO_4, 5.4 KCl, 1.8 $CaCl_2$, 0.5 $MgCl_2$, 5.4 glucose, and 5 HEPES, and pH was adjusted to 7.4 with NaOH. The internal

pipette solution contained (mM): 70 potassium aspartate, 50 KCl, 10 KH_2PO_4, 1 $MgCl_2$, 3 Na_2-ATP, 0.1 Li_2-GTP, 5 EGTA, and 5 HEPES, and pH was adjusted to 7.2 with KOH. Liquid junctional potential between the test solution and the pipette solution was measured to be around −10 mV and was corrected. HMR1556 (a kind gift from Drs. H.J. Lang and J. Pünter, Aventis Pharma Deutschland GmbH) was added from 10 mM stock solution in DMSO to the external solution (final DMSO concentration did not exceed 0.01%).

To obtain the deactivation time constant, the time course of decaying tail current at −50 mV were fitted to a single exponential function:

$$I(t) = A + B\exp(-t/\tau),$$

where I(t) means the tail current amplitude at time t, A and B are constants, and τ is the deactivation time constant.

All data are presented as mean ± standard error of the mean (SEM). Statistical analysis was performed by analysis of variance (ANOVA) followed by Tukey-Kramer post hoc comparison. Statistical significance was set at $P < 0.05$.

Cell Preparation and Confocal Imaging

For the immunofluorescence study, we constructed a hemagglutinin (HA)-tagged *KCNE3* plasmid (wild type [WT] and mutant). An HA epitope (YPYDVPDYA) was introduced into the N-terminus of *KCNE3* cDNA, using an HA-tagged 5′ primer with a KpnI restriction site at the 5′ end and a 3′ primer with BsrGI at the 3′ end. The full-length cDNA fragment of human *KCNQ1* was subcloned into pCI-neo. COS7 cells were transfected with 1.0 &mug of HA-tagged pCR3.1-*KCNE3* (WT or mutant) and 1.0 &mug of pCI-neo-*KCNQ1* plasmid in 35-mm glass-bottom dishes, using Fugene6 (Roche Diagnostics, Basel, Switzerland) according to the manufacturer's instructions. At 48λhr later, the cells were washed twice with phosphate buffered saline (PBS), followed by incubation with a mouse anti-HA primary antibody (1:500) (Covance Research Products, Inc., Berkeley, CA) for 30λminutes at 37°C. The cells were then washed twice with PBS and incubated with an anti-mouse antibody conjugated to the Alexa 488 fluorophore (1:500) (Molecular Probes, Eugene, OR) as a secondary antibody for 30λminutes at 37°C. Finally, cells were washed with and immersed in Opti-Mem, and confocal images were obtained with a Zeiss LSM 510 (Carl Zeiss GmbH, Jena, Germany).

Results

Mutation Analysis

In 485 LQTS probands, we identified two novel missense mutations and one SNP in E3 (Figs. 1 and 2). The first mutation was a single nucleotide alternation (c.296G>A) (Fig. 1A) resulting in an amino acid substitution from an arginine at residue 99 with a histidine (p.R99λH). The second mutation was a single nucleotide change (c.10A>G) (Fig. 2A), causing an amino acid substitution p.T4A, replacing a threonine at residue 4 with an alanine. This T4A missense mutation was identified in two probands. Another proband was found to have a p.P39R polymorphism, which was reported as an SNP (rs34604640: C>G). These three variants were absent in 200 unrelated healthy individuals (400 alleles) from the general Japanese population. They are located in the N-terminus (T4A and P39R) and C-terminus (R99λH), respectively. We further searched for another mutation in LQTS-related genes in these probands carrying E3 mutations (see Materials and Methods). In one of the KCNE3-T4A carriers, we identified a *KCNH2*-p.G572S mutation and in the proband with the P39R polymorphism a *KCNH2*-p.W563G mutation. SNP c.198 T>C (rs2270676), which causes no amino acid substitution (p.F66F), was identified heterozygously in roughly 20% of both LQTS probands and healthy individuals.

Phenotypic Characterization

Patient 1

The novel mutation p.R99λH was found in a 76-year-old female suffering from drug-induced TdP. Her resting 12-lead electrocardiograph (ECG) before administration of disopyramide (Fig. 1B-a) displayed sinus rhythm with normal QTc (438 ms). Because of repeated paroxysmal AF, she was started on 300λmg of disopyramide per day. At 10 days after disopyramide intake, her level of consciousness decreased and ECGs displayed frequent premature ventricular contractions (PVCs) and TdP (Fig. 1B-b). Her heart rate was 66 beats per minute (bpm), and her QTc time was prolonged to 580 ms. Serum K level was within normal range (4.0 mEq/L). Disopyramide was immediately stopped, and temporary pacing was immediately started at 90 bpm. In 3 days, TdP attacks ceased and QTc intervals returned within normal range. She had no family history of sudden cardiac death and LQTS. We did not conduct genetic analyses on the relatives of this patient, due to a lack of consent.

Patient 2

A p.T4A mutation was identified in a 16-year-old boy who had QT prolongation discovered during his school's annual health checkup. He had no history of faintness or syncope and no family history of syncope or sudden death. His resting ECG (Fig. 2B) revealed bradycardia for age (48 bpm) and QT prolongation (QTc = 525 ms). Genetic analysis on other LQTS-related genes revealed a *KCNH2*-G572S missense mutation which had been previously reported [Tester et al., 2005]. His mother and sister also remained asymptomatic but had the same heterozygous set of genetic variants (E3-T4A and *KCNH2*-G572S). Their ECGs also displayed the prolongation of QTc intervals: 520 ms and 560 ms (data not shown).

Patient 3

A p.T4A mutation was also identified in another unrelated proband, a 68-year-old female, who experienced hypokalemia-induced TdP at age 60 years. After correction of serum potassium levels, her QTc time was normalized to 430 msec (Fig. 2C). Two years after the TdP event, she was diagnosed with cardiac sarcoidosis and was started on steroid hormone therapy. Though her daughter also carried the E3-T4A mutation, she was asymptomatic with borderline QTc.

Patient 4

A p.P39R amino acid substitution was identified in a 32-year-old female who was also identified to have a novel *KCNH2* missense mutation, p.W563G. She experienced repeated episodes of late night syncope at ages 15, 21, and 26 years. Figure 3 displays her 12-lead ECG demonstrating marked QT prolongation (QTc = 512 msec) and notched T waves, suggesting LQTS type

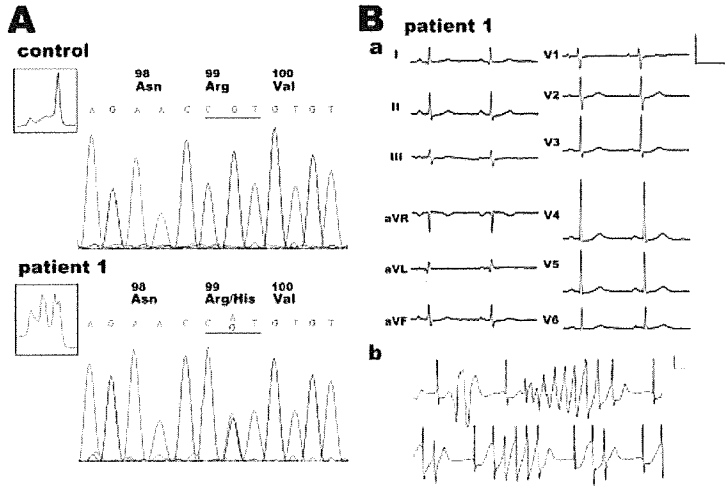

Figure 1. Molecular discovery and clinical characterization of R99H-KCNE3. **A:** DHPLC (insets) and DNA sequence analyses of normal control and Patient 1. DNA sequencing chromatograms demonstrate an arginine (Arg) to histidine (His) substitution at residue 99. **B:** ECGs of Patient 1. (a) 12-lead ECG and (b) monitoring ECG of TdP in a 76-year-old female patient. Scale bars indicate 1 mV and 400 ms. [Color figure can be viewed in the online issue, which is available at www.interscience.wiley.com.]

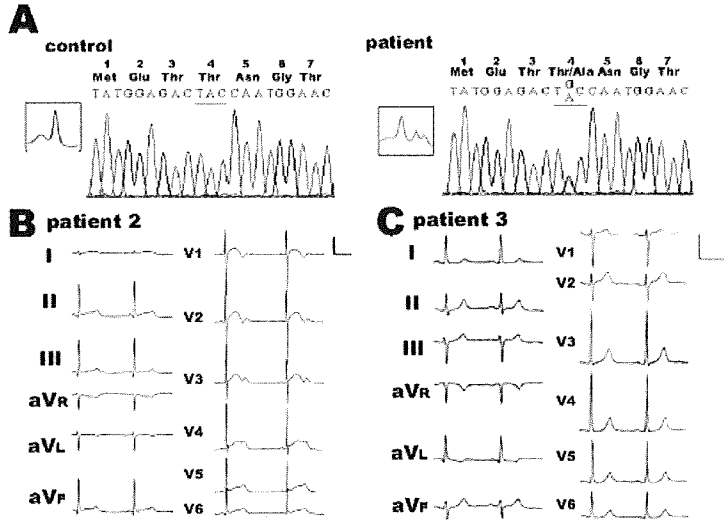

Figure 2. Molecular discovery and clinical characterization of T4A-KCNE3. **A:** DHPLC (insets) and DNA sequence analysis of normal control and patient. DNA sequencing chromatograms demonstrate a threonine (Thr) to alanine (Ala) substitution at residue 4. **B:** The 12-lead ECG of Patient 2. **C:** The 12-lead ECG of Patient 3. [Color figure can be viewed in the online issue, which is available at www.interscience.wiley.com.]

2. E3-P39R was reported as an SNP (rs34604640: C>G); however, P39R was absent in 400 control alleles from healthy Japanese cohorts. Therefore, we conducted a functional analysis of three mutants including P39R.

Biophysical Properties of KCNQ1 Channels Coexpressed With KCNE3

To clarify the functional consequences of these missense mutations (R99λH, T4A, and P39R) on E3, we assessed the biophysical properties of the mutated E3 clone by using the stably expressing human KCNQ1-CHO cell line. Figure 4A shows representative examples of whole-cell currents recorded from CHO cells stably expressing the Q1 channel transfected with or without E3 (WT or mutant). Insets to the right of each recording illustrate expanded views of the tail current elicited after return to −50 mV from test potentials. The current amplitudes were normalized by cell capacitances (current densities). Recordings from cells expressing the Q1 channel alone (left panel of Fig. 4A) displayed small amplitudes of time-dependent outward currents during depolarizing test potentials, followed by slowly deactivating tail currents on return to −50 mV. In contrast, transfection of stable Q1 cells with E3-WT (second panel in Fig. 4A) gave rise to large amplitudes of currents composed of at least two components: 1) a time-dependent outward current activated during depolarizing steps; and 2) a constitutively active background

current during depolarizing and hyperpolarizing (–50 mV) steps, as previously reported [Bendahhou et al., 2005; Schroeder et al., 2000]. After the recordings of Q1 with or without E3 current, we applied HMR1556 (1 &muM), a selective Q1 channel blocker. Though the sensitivity on the Q1 alone and Q1+E3 channel of chromanol 293B, another Q1 channel blocker, was different [Bett et al., 2006], both Q1 and Q1+E3 currents were almost totally abolished by only 1 &muM HMR1556 (lower panels of Fig. 4A).

HMR1556-sensitive current densities at the end of test pulse (Fig. 4B) were averaged from data and are plotted as the function of test voltage of Q1 (closed square), Q1+E3-WT (closed circle), Q1+E3-R99λH (open triangle), Q1+E3-T4A (open circle), and Q1+E3-P39R (closed triangle). Currents reconstituted by Q1 alone were activated at potentials greater than –40 mV, whereas those by Q1+E3 (WT and all mutants) were active at all test potentials and exhibited a strong outward rectification with a reversal potential close to E_K (–84 mV as predicted by Nernst equation). All three E3 mutants, E3-R99λH, E3-T4A, and E3-P39R, produced membrane currents with properties qualitatively similar to those of E3-WT. As summarized in Figure 4C, the current densities for the Q1+E3-R99λH current at +40 and –120 mV were 163.7±26.3 and –10.1±2.6 pA/pF, respectively. These values were significantly smaller than those of the Q1+E3-WT (301.6±33.3 pA/pF at +40 mV and –24.5±4.2 pA/pF at –120 mV, $P<0.05$). Q1+E3-T4A and Q1+E3-P39R displayed no statistically significant difference. The deactivation time constant for tail currents was significantly decreased by coexpression of E3 with Q1, but these three mutations in E3 had no significant effect on deactivation kinetics (Fig. 4D).

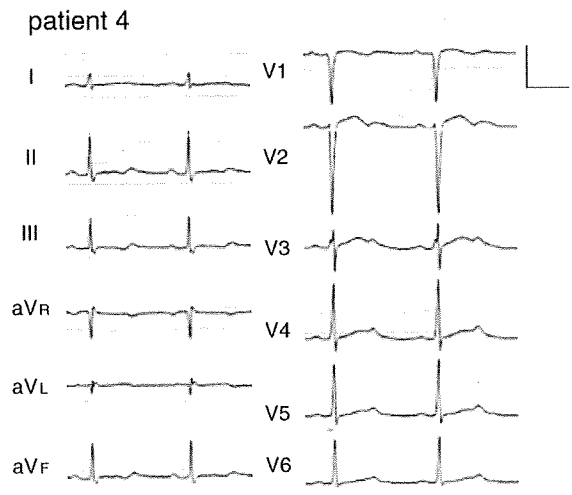

Figure 3. The 12-lead ECG of Patient 4 with QT prolongation. The patient was found to have a KCNE3-SNP, P39R, and a KCNH2-mutation, W536G.

Cellular Immunocytochemistry of KCNE3

It was reported that no E3 could be expressed on the plasma membrane in the absence of Q1 [Schroeder et al., 2000]. This was reconfirmed in our experimental protocol; the two left columns in Figure 5 show that HA-tagged E3 is not detected by Alexa 488 conjugated HA antibodies in nonpermeabilized COS7 cells in the

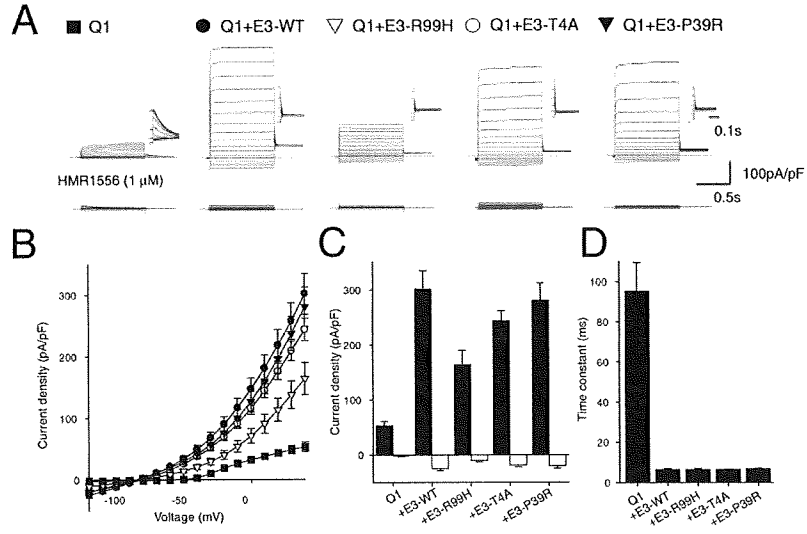

Figure 4. Functional analysis of KCNE3 and its mutants in a CHO cell line stably expressing KCNQ1 channel. **A:** Whole-cell membrane currents recorded from stable KCNQ1-CHO cells transfected without (Q1) or with KCNE3-wild type (Q1+E3-WT), KCNE3-R99λH (Q1+E3-R99λH), KCNE3-T4A (Q1+E3-T4A), or KCNE3-P39R (Q1+E3-P39R). Cells were held at –80 mV and stepped to various test potentials ranging from –120 to +40 mV in 10 mV steps for 1 sec before (upper panel) and during (lower panel) exposure to HMR1556 (1 μM). Dotted line indicates zero current level. Scale bars indicate 0.5 sec and 100 pA/pF. Insets to right of each recording illustrate expanded views of tail current elicited after return to –50 mV from test potentials. Scale bar indicates 0.1 sec. **B:** Current-voltage relationships for mean values of HMR1556-sensitive currents measured at the end of test pulses in CHO cells expressing Q1 (closed square, n = 5), Q1+E3-WT (closed circle, n = 14), Q1+E3-R99λH (open triangle, n = 12), Q1+E3-T4A (open circle, n = 12), or Q1+E3-P39R (closed triangle, n = 10). **C:** Summary of the current density measured at +40 (black bar) and –120 mV (white bar). Columns and error bars indicate mean±SEM. **D:** Deactivation time constant calculated by fitting a single exponential function to tail current at –50 mV after depolarization to +40 mV.

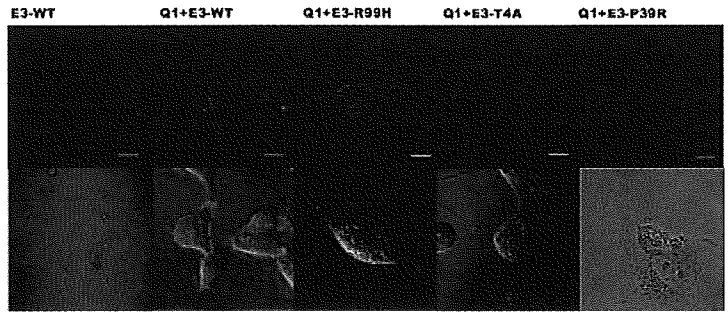

Figure 5. Cell surface expression of WT and mutant KCNE3 channels in nonpermeabilized cell. Upper panels of each column indicate HA-tagged KCNE3 (E3) (WT and three variants) with Alexa 488-conjugated antibodies with or without KCNQ1. Lower panels show merge of green fluorescence and light transmission images. Scale bars indicate 50 &mum in E3-WT and 10 &mum in others.

absence of Q1 cotransfection. In contrast, HA-tagged E3 could be visualized in the presence of Q1, which indicates that the Q1 protein is necessary for E3 to be successfully trafficked to the cell membrane. Q1 plus HA-tagged E3 channels generated currents similar to those of Q1 plus untagged E3 channels (data not shown). Figure 5 illustrates representative sets of confocal images. COS7 cells were transfected with tagged E3 (WT, T4A, and R99λH) and Q1. All Q1 plus HA-tagged E3 exhibited green fluorescence in the plasma membrane indicating that these channels were trafficked to the plasma membrane normally.

Discussion

In the present study, we report three E3 variants found in 485 LQTS probands. One of the two novel mutations, R99λH, displayed a significant decrease in outward currents when coexpressed with Q1. The proband with the E3-R99λH mutation suffered from drug-induced TdP. After washout of disopyramide, her QTc time on the ECG returned within normal range. The drug probably induced remarkable QT prolongation and TdP in the presence of a reduced repolarization reserve [Roden, 1998], which was associated with the E3-R99λH mutation.

The expression of E3 was confirmed in the human heart [Bendahhou et al., 2005; Lundquist et al., 2005, 2006]. Though neither the presence nor potential function of Q1+E3 channels in human cardiac myocytes have been determined, E3 conformed a functional channel in interaction with Q1, constitutively open potassium channel [Schroeder et al., 2000]. In addition, azimilide-sensitive Q1+E3 like currents were recorded in canine myocytes [Dun and Boyden, 2005]. On account of these results, E3 is assumed to have a physiological role in human heart. Mazhari et al. [2002] studied the effects of E3 on action potential duration (APD) in in vivo transduction of guinea pig ventricular myocytes. APD of E3-transduced myocytes was significantly reduced compared to that of control myocytes. Under the assumption that E3 might interact with KCNH2, they also performed a series of tests using an I_{Kr} blocker (E-4031) to determine whether the APD shortening was due to the interaction with E3 and KCNH2. However, E-4031 did not affect the APD in E3-transduced myocytes. As a result, the APD shortening appeared to be a result of the interaction between Q1 and E3. Although ventricular myocytes are repolarized mainly by Q1+E1 (I_{Ks}) and KCNH2 (I_{Kr}) in human hearts, we believe that the mutant E3 could prolong APD through interaction with Q1. We recently reported the knockdown of E3 expression using RNA interference in guinea pig ventricular myocytes [Toyoda et al., 2008]. The knockdown of E3 was found to prolong the APD, suggesting that E3 may play a physiological role in repolarization of cardiac action potential.

The interaction between KCNH2 and E3 is not established yet. In the experiments using *Xenopus* oocytes, KCNH2 currents were suppressed by coinjection with E3 [Schroeder et al., 2000]. On the contrary, the interaction in horse hearts could not be displayed by means of sequential immunoprecipitation and immunoblotting [Finley et al., 2002]. In addition, the I_{Kr} blocker did not affect APD in E3-transduced myocytes in guinea pigs [Mazhari et al., 2002]. Consequently, we supposed that KCNH2 plus E3 channel would affect very little for repolarization. We therefore did not pursue further examination on the interaction with KCNH2 and E3 using mammalian cell lines.

Regarding the E3-T4A mutation, we postulated that the E3-T4A has minor effects on the QT prolongation, based on the fact that no E3-T4A variant was found in our normal control. Though one of the probands had a *KCNH2*-G572S mutation [Tester et al., 2005] which is supposed to be the major reason for the QT prolongation, another proband had no mutation in major LQTS-related genes. In our biophysical assay, the mutant caused no significant difference in Q1+E3-T4A channel currents; therefore we could not display the association between E3-T4A mutation and QT prolongation. In patient 3, hypokalemia triggered the TdP, accordingly reducing extracellular potassium level may affect the currents through Q1+E3-T4A channels. Or E3 may also interact with another potassium channel alpha-subunit that affects the repolarization of cardiac myocytes, and the E3-T4A mutation may decrease the outward current to prolong QT time. We have to take into account that E3-T4A is a rare SNP, because the correlation between phenotype and genotype in our patients was not common and the number of our control was smaller compared to the studied cases.

E3-P39R may also have functional effects on repolarization. However, our proband with E3-P39R had a compound *KCNH2*-W563G mutation, as well as typical symptoms and ECG findings (Fig. 3) compatible with type 2 LQTS. In addition, functional analysis of the Q1+E3-P39R channel displayed smaller current densities than those of the Q1+E3-WT channel; however there was no statistical difference. Therefore we considered E3-P39R as a rare normal variant in Japanese.

Concerning another α subunit which interacts with KCNE3, Kv4.3 potassium channel encoded by *KCND3* produces transient outward potassium conductance (I_{to}) in the heart and KCNE3 inhibits the Kv4.3 currents [Lundby and Olesen, 2006; Radicke et al., 2006], even in the presence of KChIP2. Hence, there is a possibility that our E3 mutants affect the Kv4.3 current and prolong QT interval.

In conclusion, we identified three E3 variants among 485 Japanese LQTS probands, and one of which significantly reduced currents by interacting with Q1. Though the proband had remained asymptomatic in the absence of risk predisposing to QT prolongation, she fell into highly critical condition by taking disopyramide for AF at age of 76. Therefore, identification of E3 mutations with possible phenotypic effects provides us with information for our understanding of the mechanism of LQTS.

Acknowledgments

We thank the Japanese LQT families for their willingness to participate in this study. We are grateful to Ms. Arisa Ikeda for providing expert technical assistance, and we thank Dr. Takahiro Mitsueda for phenotypic data collection and Mr. Richard Kaszynski for reading the manuscript. W.S., Y.M., and M.H. were supported by a Health Sciences Research grant (H18-Research on Human Genome-002) from the Ministry of Health, Labour and Welfare, Japan.

References

Abbott GW, Sesti F, Splawski I, Buck ME, Lehmann MH, Timothy KW, Keating MT, Goldstein SA. 1999. MiRP1 forms I_{Kr} potassium channels with HERG and is associated with cardiac arrhythmia. Cell 97:175–187.

Abbott GW, Butler MH, Bendahhou S, Dalakas MC, Ptacek LJ, Goldstein SA. 2001. MiRP2 forms potassium channels in skeletal muscle with Kv3.4 and is associated with periodic paralysis. Cell 104:217–231.

Bendahhou S, Marionneau C, Haurogne K, Larroque MM, Derand R, Szuts V, Escande D, Demolombe S, Barhanin J. 2005. In vitro molecular interactions and distribution of KCNE family with KCNQ1 in the human heart. Cardiovasc Res 67:529–538.

Bett GC, Morales MJ, Beahm DL, Duffey ME, Rasmusson RL. 2006. Ancillary subunits and stimulation frequency determine the potency of chromanol 293B block of the KCNQ1 potassium channel. J Physiol 576(Pt 3):755–767.

Dun W, Boyden PA. 2005. Diverse phenotypes of outward currents in cells that have survived in the 5-day-infarcted heart. Am J Physiol Heart Circ Physiol 289:H667–H673.

Finley MR, Li Y, Hua F, Lillich J, Mitchell KE, Ganta S, Gilmour RF, Jr, Freeman LC. 2002. Expression and coassociation of ERG1, KCNQ1, and KCNE1 potassium channel proteins in horse heart. Am J Physiol Heart Circ Physiol 283:H126–H138.

Lundby A, Olesen SP. 2006. KCNE3 is an inhibitory subunit of the Kv4.3 potassium channel. Biochem Biophys Res Commun 346:958–967.

Lundby A, Ravn LS, Svendsen JH, Hauns S, Olesen SP, Schmitt N. 2008. KCNE3 mutation V17λM identified in a patient with lone atrial fibrillation. Cell Physiol Biochem 21:47–54.

Lundquist AL, Manderfield LJ, Vanoye CG, Rogers CS, Donahue BS, Chang PA, Drinkwater DC, Murray KT, George AL, Jr. 2005. Expression of multiple KCNE genes in human heart may enable variable modulation of I_{Ks}. J Mol Cell Cardiol 38:277–287.

Lundquist AL, Turner CL, Ballester LY, George AL, Jr. 2006. Expression and transcriptional control of human KCNE genes. Genomics 87:119–128.

Mazhari R, Nuss HB, Armoundas AA, Winslow RL, Marban E. 2002. Ectopic expression of KCNE3 accelerates cardiac repolarization and abbreviates the QT interval. J Clin Invest 109:1083–1090.

Morin TJ, Kobertz WR. 2007. A derivatized scorpion toxin reveals the functional output of heteromeric KCNQ1-KCNE K^+ channel complexes. ACS Chem Biol 2:469–473.

Moss AJ, Kass RS. 2005. Long QT syndrome: from channels to cardiac arrhythmias. J Clin Invest 115:2018–2024.

Ohno S, Zankov DP, Yoshida H, Tsuji K, Makiyama T, Itoh H, Akao M, Hancox JC, Kita T, Horie M. 2007. N- and C-terminal KCNE1 mutations cause distinct phenotypes of long QT syndrome. Heart Rhythm 4:332–340.

Radicke S, Cotella D, Graf EM, Banse U, Jost N, Varro A, Tseng GN, Ravens U, Wettwer E. 2006. Functional modulation of the transient outward current Ito by KCNE beta-subunits and regional distribution in human non-failing and failing hearts. Cardiovasc Res 71:695–703.

Roden DM. 1998. Taking the "idio" out of "idiosyncratic": predicting torsades de pointes. Pacing Clin Electrophysiol 21:1029–1034.

Schroeder BC, Waldegger S, Fehr S, Bleich M, Warth R, Greger R, Jentsch TJ. 2000. A constitutively open potassium channel formed by KCNQ1 and KCNE3. Nature 403:196–199.

Tester DJ, Will ML, Haglund CM, Ackerman MJ. 2005. Compendium of cardiac channel mutations in 541 consecutive unrelated patients referred for long QT syndrome genetic testing. Heart Rhythm 2:507–517.

Toyoda F, Ueyama H, Ding WG, Matsuura H. 2006. Modulation of functional properties of KCNQ1 channel by association of KCNE1 and KCNE2. Biochem Biophys Res Commun 344:814–820.

Toyoda F, Zankov DP, Ding WG, Matsuura H. 2008. Functional regulation of cardiac KCNQ1 potassium channel by association of KCNE3. [Abstract]. 2008 Biophysics Society Meeting Abstracts, February 2–6, 2008. Biophys J 94(Suppl):3025.

KCNE2 modulation of Kv4.3 current and its potential role in fatal rhythm disorders

Jie Wu, PhD,* Wataru Shimizu, MD, PhD,† Wei-Guang Ding, MD, PhD,‡ Seiko Ohno, MD, PhD,§ Futoshi Toyoda, PhD,‡ Hideki Itoh, MD, PhD,¶ Wei-Jin Zang, MD, PhD,* Yoshihiro Miyamoto, MD, PhD,‖ Shiro Kamakura, MD, PhD,† Hiroshi Matsuura, MD, PhD,‡ Koonlawee Nademanee, MD, FACC,# Josep Brugada, MD,** Pedro Brugada, MD,†† Ramon Brugada, MD, PhD, FACC,‡‡ Matteo Vatta, PhD,§§¶¶ Jeffrey A. Towbin, MD, FAAP, FACC,§§ Charles Antzelevitch, PhD, FACC, FAHA, FHRS,‖‖ Minoru Horie, MD, PhD¶

*From the *Pharmacology Department, Medical School of Xi'an Jiaotong University. Xi'an, Shaanxi, China, †Division of Cardiology, Department of Internal Medicine, National Cardiovascular Center, Suita, Japan, ‡Department of Physiology, Shiga University of Medical Science, Ohtsu, Japan, §Department of Cardiovascular Medicine, Kyoto University of Graduate School of Medicine, Kyoto, Japan, ¶Department of Cardiovascular Medicine, Shiga University of Medical Science, Shiga, Japan, ‖Laboratory of Molecular Genetics, National Cardiovascular Center, Suita, Japan, #Department of Medicine (Cardiology), University of Southern California, Los Angeles, California, **Cardiovascular Institute, Hospital Clinic, University of Barcelona, Barcelona, Spain, ††Heart Rhythm Management Centre, Free University of Brussels (UZ Brussel) VUB, Brussels, Belgium, ‡‡School of Medicine, Cardiovascular Genetics Center, University of Girona, Girona, Spain, §§Departments of Pediatrics, Baylor College of Medicine, Houston, Texas, ¶¶Department of Molecular Physiology and Biophysics, Baylor College of Medicine, Houston, Texas, and ‖‖Masonic Medical Research Laboratory, Utica, New York.*

BACKGROUND The transient outward current I_{to} is of critical importance in regulating myocardial electrical properties during the very early phase of the action potential. The auxiliary β subunit *KCNE2* recently was shown to modulate I_{to}.

OBJECTIVE The purpose of this study was to examine the contributions of *KCNE2* and its two published variants (M54T, I57T) to I_{to}.

METHODS The functional interaction between Kv4.3 (α subunit of human I_{to}) and wild-type (WT), M54T, and I57T *KCNE2*, expressed in a heterologous cell line, was studied using patch-clamp techniques.

RESULTS Compared to expression of Kv4.3 alone, co-expression of WT *KCNE2* significantly reduced peak current density, slowed the rate of inactivation, and caused a positive shift of voltage dependence of steady-state inactivation curve. These modifications rendered Kv4.3 channels more similar to native cardiac I_{to}. Both M54T and I57T variants significantly increased I_{to} current density and slowed the inactivation rate compared with WT *KCNE2*. Moreover, both variants accelerated the recovery from inactivation.

CONCLUSION The study results suggest that *KCNE2* plays a critical role in the normal function of the native I_{to} channel complex in human heart and that M54T and I57T variants lead to a gain of function of I_{to}, which may contribute to generating potential arrhythmogeneity and pathogenesis for inherited fatal rhythm disorders.

KEYWORDS Cardiac arrhythmia; M54T variation; I57T variation; *KCNE2*; Kv4.3; Sudden cardiac death

ABBREVIATIONS CHO = Chinese hamster ovary; **HERG** = human ether-a-go-go related gene; **WT** = wild type

(Heart Rhythm 2010;7:199–205)

Introduction

Classic voltage-gated K^+ channels consist of four pore-forming (α) subunits that contain the voltage sensor and ion selectivity filter[1,2] and accessory regulating (β) subunits.[3] *KCNE* family genes encode several kinds of β subunits consisting of single transmembrane-domain peptides that co-assemble with α subunits to modulate ion selectivity, gating kinetics, second messenger regulation, and the pharmacology of K^+ channels. Association of the *KCNE1* product minK with the α subunit Kv7.1 encoding *KCNQ1* forms the slowly activating delayed rectifier K^+ current I_{Ks} in the heart.[4,5] In contrast, association of the *KCNE2* product MiRP1 with the human ether-a-go-go related gene (HERG) forms the cardiac rapid delayed rectifier K^+ current I_{Kr}.[6]

The first two authors contributed equally to the original concept and the authorship of this study. This study was supported by grants from the Ministry of Education, Culture, Sports, Science, Technology Leading Project for Biosimulation to Dr. Horie; Health Sciences Research grants (H18-Research on Human Genome-002) from the Ministry of Health, Labour and Welfare, Japan to Drs. Shimizu and Horie; the National Natural Science Foundation of China (Key Program, No.30930105; General Program, No. 30873058, 30770785) and the National Basic Research Program of China (973 Program, No. 2007CB512005) and CMB Distinguished Professorships Award (No. F510000/G16916404) to Dr. Zang; and National Institutes of Health Grant HL47678 and Free and Accepted Masons of New York State and Florida to Dr. Antzelevitch. **Address reprint requests and correspondence:** Dr. Minoru Horie, Department of Cardiovascular and Respiratory Medicine, Shiga University of Medical Science, Otsu, Shiga 520-2192, Japan. E-mail address: horie@belle.shiga-med.ac.jp. (Received August 20, 2009; accepted October 7, 2009.)

1547-5271/$ -see front matter doi:10.1016/j.hrthm.2009.10.012

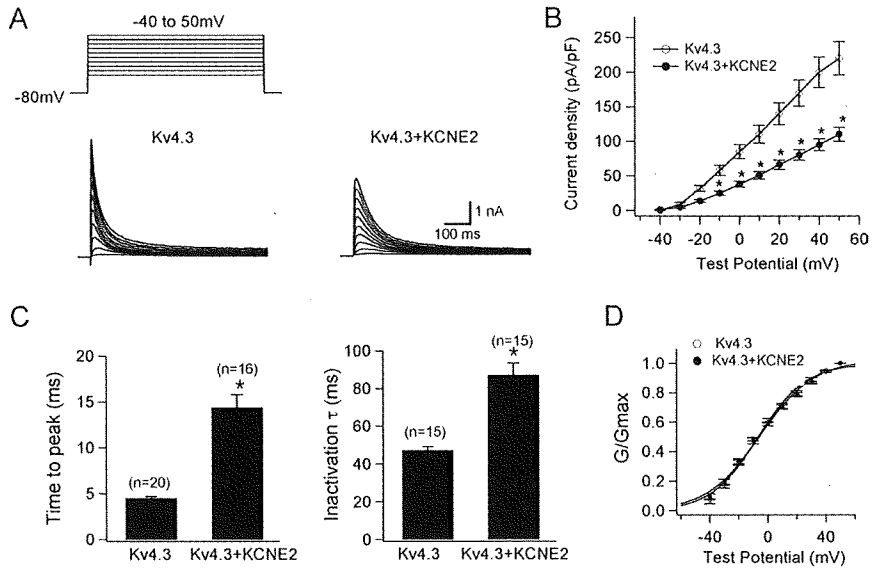

Figure 1 *KCNE2* co-expression with Kv4.3 produces smaller I_{to}-like currents with slower activation/inactivation kinetics. **A:** Representative current traces recorded from Chinese hamster ovary (CHO) cells expressing Kv4.3 **(left)** and Kv4.3 + *KCNE2* **(right).** As shown in the **inset** in panel A, depolarizing step pulses of 1-second duration were introduced from a holding potential of −80 mV to potentials ranging from −40 to +50 mV in 10-mV increments. **B:** Current–voltage relationship curve showing peak current densities in the absence and presence of co-transfected *KCNE2* (*P <.05 vs Kv4.3). **C:** Bar graphs showing the kinetic properties of reconstituted channel currents: time to peak of activation course **(left)** and inactivation time constants **(right)** measured using test potential to +20 mV (*P <.05 vs Kv4.3). Numbers in parentheses indicate numbers of experiments. **D:** Normalized conductance–voltage relationship for peak outward current of Kv4.3 and Kv4.3 + *KCNE2* channels.

Abbott et al reported that three *KCNE2* variants (Q9E, M54T, I57T) caused a loss of function in I_{Kr} and thereby were associated with the congenital or drug-induced long QT syndrome.[6,7] However, the reported QTc values in two index patients with M54T and I57T variants, both located in the transmembrane segment of MiRP1, were only mildly prolonged (390–500 ms and 470 ms).[6] We recently identified the same missense *KCNE2* variant, I57T, in which isoleucine was replaced by threonine at codon 57, in three unrelated probands showing a Brugada type 1 ECG. These findings are difficult to explain on the basis of a loss of function in I_{Kr}, thus leading us to explore other mechanisms.

Recent studies have demonstrated that interaction between α and β subunits (*KCNE*s) of voltage-gated K^+ channel is more promiscuous; for example, MiRP1 has been shown to interact with Kv7.1,[8–10] HCN1,[11] Kv2.1,[12] and Kv4.2.[13] These studies suggest that MiRP1 may also co-associate with Kv4.3 and contribute to the function of transient outward current (I_{to}) channels.[14] Indeed, a recent study reported that I_{to} is diminished in *kcne2* (–/–) mice.[15]

In the human heart, I_{to} currents are of critical importance in regulating myocardial electrical properties during the very early phase of the action potential and are thought to be central to the pathogenesis of Brugada-type ECG manifestations.[16] Antzelevitch et al demonstrated that a gain of function in I_{to} secondary to a mutation in *KCNE3* contributes to a Brugada phenotype by interacting with Kv4.3 and thereby promoting arrhythmogenicity.[14]

We hypothesized that mutations in *KCNE2* may have similar actions and characterize the functional consequences of interaction of wild-type (WT) and two mutant (I57T, M54T) MiRP1 with Kv4.3[17,18] using heterologous co-expression of these α and β subunits in Chinese hamster ovary (CHO) cells.

Methods

Heterologous expression of hKv4.3 and β subunits in CHO cells

Full-length cDNA fragment of *KCNE2* in pCR3.1 vector[10] was subcloned into pIRES-CD8 vector. This expression vector is useful in cell selection for later electrophysiologic study (see below). Two *KCNE2* mutants (M54T, I57T) were constructed using a Quick Change II XL site-directed mutagenesis kit according to the manufacturer's instructions (Stratagene, La Jolla, CA, USA) and subcloned to the same vector. Two *KCNE2* mutants were fully sequenced (ABI3100x, Applied Biosystems, Foster City, CA, USA) to ensure fidelity. Full-length cDNA encoding the short isoform of human Kv4.3 subcloned into the pIRES-GFP (Clontech, Palo Alto, CA, USA) expression vector was kindly provided by Dr. G.F. Tomaselli (Johns Hopkins University). Full-length cDNA encoding Kv channel-interacting protein (*KCNIP2*) subcloned into the PCMV-IRS expression vector was a kind gift from Dr. G.-N. Tseng (Virginia Commonwealth University). *KCND3* was transiently transfected into CHO cells together with *KCNE2* (or M54T or I57T) cDNA at equimolar ratio (*KCND3* 1.5 μg,

Table 1 Effects of *KCNE2* on Kv4.3 and Kv4.3 + KChIP2b

Parameter	Kv4.3	Kv4.3 *KCNE2*	Kv4.3 KChIP2b	Kv4.3 KChIP2b *KCNE2*
Current density at +20 mV (pA/pF)	142.0 ± 16.0 (n = 12)	66.0 ± 6.6* (n = 12)	191.5 ± 33.8 (n = 15)	77.8 ± 5.9† (n = 20)
Steady-state activation ($V_{0.5}$ in mV)	−6.5 ± 2.1 (n = 9)	−5.5 ± 1.7 (n = 11)	−7.5 ± 1.7 (n = 8)	−7.4 ± 1.4 (n = 8)
Steady-state inactivation ($V_{0.5}$ in mV)	−46.0 ± 1.3 (n = 10)	−40.8 ± 1.7* (n = 8)	−49.8 ± 1.4 (n = 7)	−44.5 ± 1.9† (n = 7)
τ of inactivation at +20 mV (τ_{inact} in ms)	47.3 ± 2.0 (n = 15)	87.2 ± 6.2* (n = 15)	47.5 ± 2.2 (n = 15)	66.6 ± 3.5† (n = 15)
Time to peak at +50 mV (TtP in ms)	4.5 ± 0.2 (n = 20)	14.4 ± 1.4* (n = 16)	4.1 ± 0.2 (n = 15)	6.1 ± 0.5† (n = 21)
τ of recovery from inactivation (ms)	419.6 ± 18.8 (n = 6)	485.6 ± 74.8 (n = 6)	89.2 ± 5.3 (n = 6)	60.2 ± 6.9† (n = 6)

*Significantly different from Kv4.3.
†Significantly different from Kv4.3 + KChIP2b.

KCNE2 1.5 μg) using Lipofectamine (Invitrogen Life Technologies, Carlsbad, CA, USA) according to the manufacturer's instructions. In one set of experiments, we also co-transfected equimolar levels of KChIP2b (*KCND3* 1.5 μg, *KCNE2* 1.5 μg, *KCNIP2* 1.5 μg). The transfected cells were then cultured in Ham's F-12 medium (Nakalai Tesque, Inc., Kyoto, Japan) supplemented with 10% fetal bovine serum (JRH Biosciences, Inc., Lenexa, KS, USA) and antibiotics (100 international units per milliliter penicillin and 100 μg/mL streptomycin) in a humidified incubator gassed with 5% CO_2 and 95% air at 37°C. The cultures were passaged every 4 to 5 days using a brief trypsin-EDTA treatment. The trypsin-EDTA treated cells were seeded onto glass coverslips in a Petri dish for later patch-clamp experiments.

Electrophysiologic recordings and data analysis

After 48 hours of transfection, a coverslip with cells was transferred to a 0.5-mL bath chamber at 25°C on an inverted microscope stage and perfused at 1 to 2 mL/min with extracellular solution containing the following (in mM): 140 NaCl, 5.4 KCl, 1.8 $CaCl_2$, 0.5 $MgCl_2$, 0.33 NaH_2PO_4, 5.5 glucose, and 5.0 HEPES; pH 7.4 with NaOH. Cells that emitted green fluorescence were chosen for patch-clamp experiments. If co-expressed with *KCNE2* (or its mutants), the cells were incubated with polystyrene microbeads precoated with anti-CD8 antibody (Dynabeads M450, Dynal, Norway) for 15 minutes. In these cases, cells that emitted green fluorescence and had attached beads were chosen for electrophysiologic recording. Whole-cell membrane currents were recorded with an EPC-8 patch-clamp amplifier (HEKA, Lambrecht, Germany), and data were low-pass filtered at 1 kHz, acquired at 5 kHz through an LIH-1600 analog-to-digital converter (HEKA), and stored on hard disk using PulseFit software (HEKA). Patch pipettes were fabricated from borosilicate glass capillaries (Narishige, Tokyo, Japan) using a horizontal microelectrode puller (P-97, Sutter Instruments, Novato, CA, USA) and the pipette tips fire-polished using a microforge. Patch pipettes had a resistance of 2.5 to 5.0 MΩ when filled with the following pipette solution (in mM): 70 potassium aspartate, 50 KCl, 10 KH_2PO_4, 1 $MgSO_4$, 3 Na_2-ATP (Sigma, Japan, Tokyo), 0.1 Li_2-GTP (Roche Diagnostics GmbH, Mannheim, Germany), 5 EGTA, and 5 HEPES (pH 7.2).

Cell membrane capacitance (C_m) was calculated from 5 mV-hyperpolarizing and depolarizing steps (20 ms) applied from a holding potential of −80 mV according to Equation 1[19]:

$$C_m = \tau_c I_0/\Delta V_m(1 - I_\infty/I_0), \quad (1)$$

where τ_c = time constant of capacitance current relaxation, I_0 = initial peak current amplitude, ΔV_m = amplitude of voltage step, and I_∞ = steady-state current value. Whole-cell currents were elicited by a family of depolarizing voltage steps from a holding potential of −80 mV. The difference between the peak current amplitude and the current at the end of a test pulse (1-second duration) was referred to as the transient outward current. To control for cell size variability, currents were expressed as densities (pA/pF).

Steady-state activation curves were obtained by plotting the normalized conductance as a function of peak outward potentials. Steady-state inactivation curves were generated by a standard two-pulse protocol with a conditioning pulse of 500-ms duration and obtained by plotting the normalized current as a function of the test potential. Steady-state inactivation/activation kinetics were fitted to the following Boltzmann equation (Eq. 2):

$$Y(V) = 1/(1 + \exp[(V_{1/2} - V)/k]), \quad (2)$$

where Y = normalized conductance or current, $V_{1/2}$ = potential for half-maximal inactivation or activation, respectively, and k = slope factor.

Data relative to inactivation time constants, time to peak, and mean current levels were obtained by using current data recorded at +50 mV or +20 mV. Recovery from inactivation was assessed by a standard paired-pulse protocol: a 400-ms test pulse to +50 mV (P1) followed by a variable

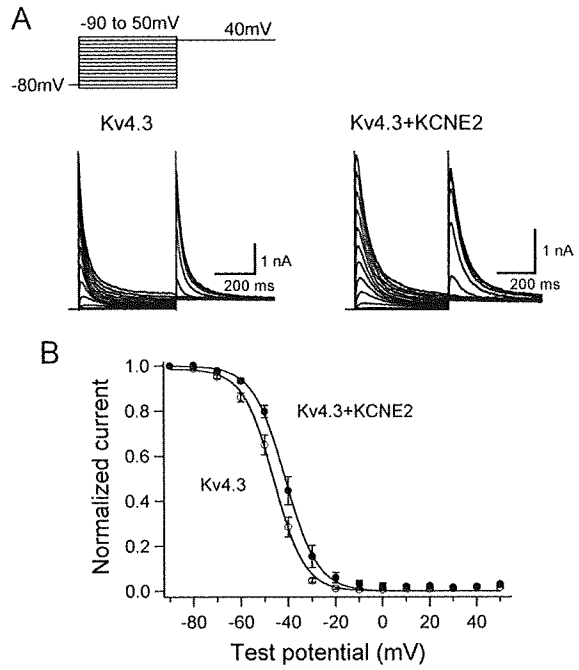

Figure 2 *KCNE2* co-expression with Kv4.3 causes a positive shift of voltage dependence of steady-state inactivation. **A:** Representative Kv4.3 and Kv4.3 + *KCNE2* current traces induced by 500-ms pulses (P1) from −90 to +50 mV applied from the holding potential −80 mV in 10-mV steps followed by a second pulse (P2) to +40 mV. **B:** Steady-state inactivation curves for Kv4.3 *(open circles)* and Kv4.3 + *KCNE2 (closed circles)* channels.

recovery interval at −80 mV and then a second test pulse to +50 mV (P2). Both the inactivation time constants and the time constant for recovery from inactivation were determined by fitting the data to a single exponential (Eq. 3):

$$I(t) \text{ (or P2/P1)} = A + B_{exp}(-t/\tau), \quad (3)$$

where I(t) = current amplitude at time t, A and B = constants, and τ = inactivation time constant or time constant for recovery from inactivation. For measurement of recovery from inactivation, the plot of P2/P1 instead of I(t) was used.

All data were given as mean ± SEM. Statistical comparisons between two groups were analyzed using Student's unpaired t-test. Comparisons among multiple groups were analyzed using analysis of variance followed by Dunnett test. $P < .05$ was considered significant.

Results

Effects of *KCNE2* on Kv4.3 currents and its gating kinetics

WT *KCNE2* initially was co-expressed with *KCND3*, the gene encoding Kv4.3, the α subunit of the I_{to} channel,[17,18] in CHO cells. Figure 1A shows representative whole-cell current traces recorded from cells transfected with *KCND3* and co-transfected with (right) or without (left) *KCNE2*. Cells expressing Kv4.3 channels alone showed rapidly activating and inactivating currents. Co-expression of *KCNE2* significantly reduced peak current densities as summarized in the current–voltage relationship curve shown in Figure 1B and slowed both activation and inactivation kinetics (Table 1). Figure 1C (left) shows mean time intervals from the onset of the pulse to maximum current (time to peak), whereas the right panel shows time constants of inactivation (at +20 mV) obtained using Equation 3. Thus, co-transfection of *KCNE2* significantly increased both the time to peak and the time constant.

In contrast, *KCNE2* did not affect the voltage dependence of steady-state activation as assessed by plotting the normalized conductance as a function of test potential (Figure 1D). Fitting to the Boltzmann equation (Eq. 2) yielded half-maximal activation potentials of −6.5 ± 2.1 mV for Kv4.3 alone (open circles) and −5.5 ± 1.7 mV for Kv4.3 + *KCNE2* channels (filled circles, P = NS; Table 1). These findings are consistent with those previously reported for studies using *Xenopus* oocytes, CHO cells, and HEK293 cells.[20,21]

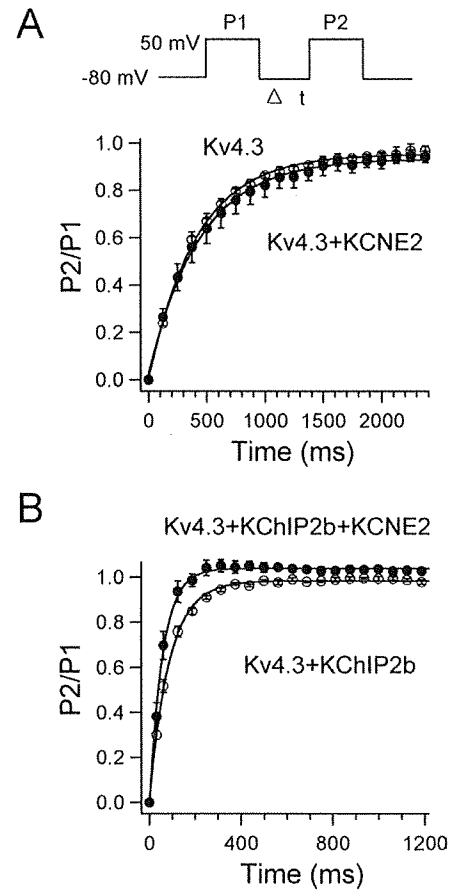

Figure 3 Effects of *KCNE2* co-expression on recovery from inactivation of Kv4.3 **(A)** and Kv4.3 + KChIP2b **(B)** currents. Recovery from inactivation was assessed by a two-pulse protocol **(A, inset):** a 400-ms test pulse to +50 mV (P1) followed by a variable interval at −80 mV, then by a second test pulse to +50 mV (P2). Data were fit to a single exponential.

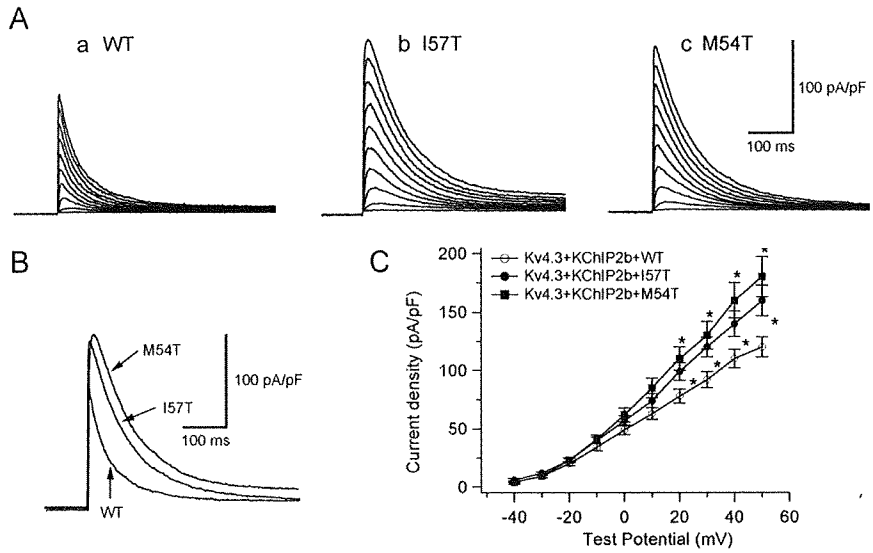

Figure 4 Two *KCNE2* transmembrane variants, I57T and M54T, increase the reconstituted Kv4.3 + KChIP2b channel current and slow its inactivation. **A:** Three sets of current traces elicited by depolarizing pulses for 500 ms from a holding potential of −80 mV to potentials ranging between −40 and +50 mV in 10-mV increments (same protocol as in experiments of Figure 1A). **B:** Superimposition of three original current traces recorded upon depolarization showing variant-related increase in peak outward current density. **C:** Current–voltage relationship curve showing average peak outward current densities (*P <.05 vs Kv4.3 + KChIP2b + WT). WT = wild type.

KCNE2 co-expression also caused a positive shift (approximately +5 mV) of voltage dependence of steady-state inactivation. Steady-state inactivation was assessed using a double-step pulse method (Figure 2A, inset). Peak outward currents recorded at various levels of prepulse (Figure 2A) were normalized by that measured after a 500-ms prepulse at −90 mV and are plotted as a function of prepulse test potentials (Figure 2B). Half-inactivation potentials of steady-state inactivation, determined by fitting data to the Boltzmann equation (Eq. 2), were −46.0 ± 1.3 mV for Kv4.3 (open circles) and −40.8 ± 1.7 mV for Kv4.3 + *KCNE2* (filled circles, P <.01), consistent with the observation of Tseng's group.[13]

A double-pulse protocol (Figure 3A, inset) was used to test the effect of *KCNE2* co-expression on the time course for recovery from inactivation. Figure 3A shows the time course of recovery of Kv4.3 alone (open circles) and Kv4.3 + *KCNE2* (filled circles). Mean time constants for recovery from inactivation were not significantly different, indicating that co-transfection of *KCNE2* did not affect the time course of recovery from inactivation.

Effects of *KCNE2* on Kv4.3 + KChIP2b current and its gating kinetics

For human native cardiac I_{to}, KChIP2 has been shown to serve as a principal β subunit.[22–25] Accordingly, in another series of experiments, we examined the effect of WT and mutant *KCNE2* on Kv4.3 + KChIP2b current. Consistent with previous reports, in the presence of KChIP2, Kv4.3 currents showed a significantly faster recovery from inactivation (Figure 3B and Table 1).[26,27] Co-expression of WT *KCNE2* produced similar changes on Kv4.3 + KChIP2b current as on Kv4.3 current (Table 1). Kv4.3 + KChIP2b current recovery from inactivation was further accelerated: average time constant was 89.2 ± 6.5 ms for Kv4.3 + KChIP2b alone (open circles) and 60.2 ± 8.4 ms for Kv4.3 + KChIP2b + *KCNE2* (filled circles, P <.05). In 16 of 21 cells transfected with *KCNE2*, we observed an "overshoot" phenomenon, which is commonly seen during recording of native I_{to} in human ventricular myocytes.[28]

KCNE2 variants increase Kv4.3 + KChIP2b current and alter its gating kinetics

The I57T variant was first identified in an asymptomatic middle-aged woman with very mild QT prolongation.[6] In addition to this variant, the authors reported another *KCNE2* variant of the transmembrane segment (M54T) that was associated with ventricular fibrillation during exercise in a middle-aged woman. This patient appeared to show a wide range of QTc interval (390–500 ms). Therefore, we tested the functional effects of these two transmembrane *KCNE2* variants on Kv4.3 + KChIP2b currents.

The three panels of Figure 4A show three sets of current traces elicited by depolarizing pulses from a holding potential of −80 mV in cells co-transfected with WT (a), I57T (b), or M54T (c) *KCNE2*. Neither variant caused a significant shift of half-maximal activation voltage: −7.4 ± 1.4 mV (n = 8) for co-expression of WT *KCNE2*, −6.1 ± 1.5 mV (n = 8) for I57T, and −6.6 ± 1.6 mV (n = 8) for M54T. Both variants significantly increased I_{to} density: 125.0 ± 10.6 pA/pF in WT *KCNE2* (n = 21), 178.1 ± 12.1 pA/pF with I57T (n = 9), and 184.3 ± 27.9 pA/pF with M54T (n = 9, Figure 4C).

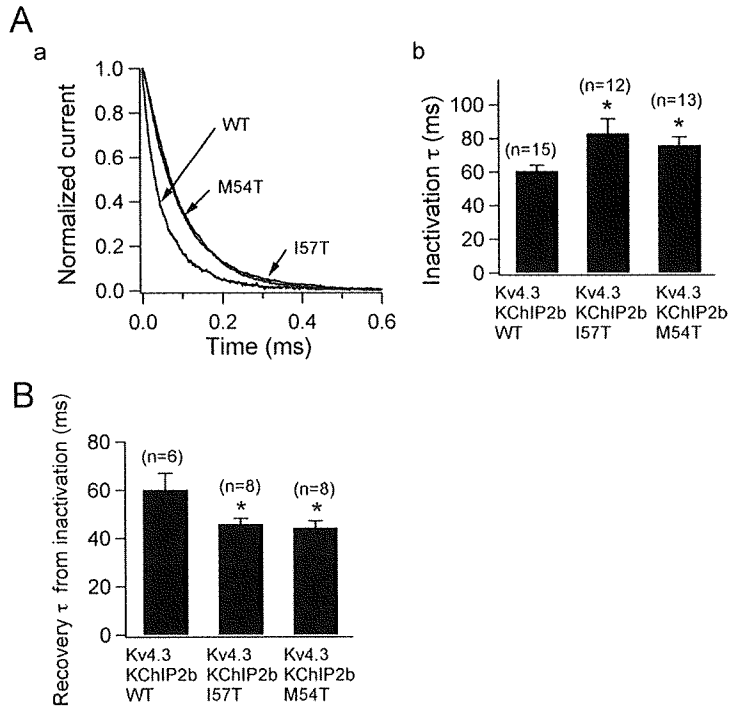

Figure 5 Two *KCNE2* variants slow inactivation kinetics and accelerate recovery from inactivation. **A, a:** Three current traces obtained from Chinese hamster ovary (CHO) cells transfected with wild-type (WT), I57T, and M54T *KCNE2* variant co-expressed with Kv4.3 and KChIP2b. Traces, which are normalized and superimposed, show that the variants slow inactivation. **A, b:** Time constants of decay at +20 mV for WT and variant *KCNE2* (*P <.05 vs Kv4.3 + KChIP2b + WT). Numbers in parentheses indicate numbers of observations. **B:** Time constants of recovery from inactivation recorded using a double-pulse protocol (*P <.05 vs Kv4.3 + KChIP2b + WT). Numbers in parentheses indicate numbers of observations.

Figure 5A shows the three traces depicted in Figure 4B normalized to their peak current level. This representation shows that the time course of inactivation of the two variant currents is slowed. The current decay was fitted by Equation 3 and the time constants (at +20 mV) summarized in Figure 5A, panel b. Finally, Figure 5B shows that the time constants of recovery of the two mutant channels from inactivation were significantly reduced. Thus, compared to WT *KCNE2*, recovery of reconstituted Kv4.3 + KChIP2b channels from inactivation was significantly accelerated with both I57T and M54T mutants.

Discussion

Kv4.3/KChIP2/MiRP1 complex can recapitulate the native I_{to}

In the present study, co-expression of WT *KCNE2* produced changes in kinetic properties (Figures 1–3 and Table 1) that led to close recapitulation of native cardiac I_{to}.[28,29] Notably, in addition to causing a positive shift of steady-state inactivation (Figure 2), *KCNE2* co-expression hastened the recovery of Kv4.3 + KChIP2b channels from inactivation (Figure 3). These modifications rendered Kv4.3 + KChIP2b channels more similar to native cardiac I_{to}, suggesting that *KCNE2* may be an important component of the native I_{to} channel complex. In contrast to a previous observation in HEK293 cells,[21] *KCNE2* co-expression decreased the current density of Kv4.3 and Kv4.3 + KChIP2b channel current in the present study, which seems to be a more reasonable result as the native I_{to} density reportedly was smaller in isolated human heart.[28] *KCNE2* co-expression has also been shown to reduce the density of Kv7.1[8,9] and HERG[6,7] channels.

Similar to the result of Deschenes and Tomaselli,[21] we failed to observe an overshoot during recovery from inactivation when *KCNE2* was co-expressed with Kv4.3 (Figure 3A), which is in contrast to the report of another group.[13] However, co-expression of *KCNE2* with Kv4.3 + KChIP2 channels produced an overshoot (Figure 3B), consistent with the report of Wettwer's group.[25] Wettwer et al also found that other *KCNE* subunits either were ineffective or induced only a small overshoot in CHO cells. Therefore, both MiRP1 and KChIP2 subunits are sufficient and necessary to recapitulate native I_{to} in the heart. Considering that the overshoot phenomenon has been described only in human ventricular I_{to} channels of the epicardial but not endocardial region,[28] these results may further implicate participation of MiRP1 and KChIP2 in the I_{to} channel complex in epicardium.

KCNE2 variants may alter the arrhythmogenic substrate by modulating I_{to}

Heterologous expression in CHO cells was conducted to examine the functional effects of I57T and M54T variants on Kv4.3 + KChIP2 channels. Both I57T and M54T

KCNE2 variants significantly (1) increased peak transient outward current density (Figure 4), (2) slowed the decay of the reconstituted I_{to} (Figure 5A), and (3) accelerated its recovery from inactivation (Figure 5B). Both variants thus caused an important gain of function in human I_{to}. These sequence changes may play a role in modulating I_{to} and thereby predispose to some inherited fatal rhythm disorders.

Functional effects on I_{to} induced by I57T and M54T resemble each other, increasing I_{to} density and accelerating its recovery from inactivation. The gain of function in I_{to} opposes the fast inward Na^+ currents during phase 0 of the action potential, leading to all or none repolarization at the end of phase 1 and loss of the epicardial action potential dome, thus promoting phase 2 reentry and fatal ventricular arrhythmias.[30]

Another *KCNE2* variant (M54T) associated with fatal arrhythmias was first identified in a woman who had a history of ventricular fibrillation and varied QT intervals.[6] It is possible that her arrhythmia was also related to a gain of function in I_{to} secondary to this variation in *KCNE2*. Interestingly, the I57T variant has been reported to produce a loss of function of HERG or Kv7.1 channels, thereby predisposing to long QT syndrome,[6,8] indicating that the same *KCNE2* variant could cause two different cardiac rhythm disorders, similar to long QT syndrome and Brugada syndrome caused by *SCN5A* mutations.[31,32]

References

1. Kass RS, Freeman LC. Potassium channels in the heart: cellular, molecular, and clinical implications. Trends Cardiovasc Med 1993;3:149–159.
2. MacKinnon R. Determination of the subunit stoichiometry of a voltage-activated potassium channel. Nature 1991;350:232–235.
3. Abbott GW, Goldstein SA. A superfamily of small potassium channel subunits: form and function of the MinK-related peptides (MiRPs). Q Rev Biophys 1998;31:357–398.
4. Barhanin J, Lesage F, Guillemare E, Fink M, Lazdunski M, Romey G. KvLQT1 and IsK (minK) proteins associate to form the I_{Ks} cardiac potassium current. Nature 1996;384:78–80.
5. Sanguinetti MC, Curran ME, Zou AR, et al. Coassembly of KvLQT1 and minK (I_{Ks}) proteins to form cardiac I_{Ks} potassium channel. Nature 1996: 384:80–83.
6. Abbott GW, Sesti F, Splawski I, et al. MiRP1 forms I_{Kr} potassium channels with HERG and is associated with cardiac arrhythmia. Cell 1999;97:175–187.
7. Sesti F, Abbott GW, Wei J, et al. A common polymorphism associated with antibiotic-induced cardiac arrhythmia. Proc Natl Acad Sci U S A 2000;97: 10613–10618.
8. Tinel N, Diochot S, Borsotto M, Lazdunski M, Barhanin J. *KCNE2* confers background current characteristics to the cardiac KCNQ1 potassium channel. EMBO J 2000;19:6326–6330.
9. Wu DM, Jiang M, Zhang M, Liu XS, Korolkova YV, Tseng GN. *KCNE2* is colocalized with KCNQ1 and *KCNE1* in cardiac myocytes and may function as a negative modulator of $I_{(Ks)}$ current amplitude in the heart. Heart Rhythm 2006;3:1469–1480.
10. Toyoda F, Ueyama H, Ding WG, Matsuura H. Modulation of functional properties of KCNQ1 channel by association of KCNE1 and KCNE2. Biochem Biophys Res Commun 2006;344:814–820.
11. Yu H, Wu J, Potapova I, et al. MinK-related peptide 1: a beta subunit for the HCN ion channel subunit family enhances expression and speeds activation. Circ Res 2001;88:E84–E87.
12. McCrossan ZA, Roepke TK, Lewis A, Panaghie G, Abbott GW. Regulation of the Kv2.1 potassium channel by MinK and MiRP1. J Membr Biol 2009;228:1–14.
13. Zhang M, Jiang M, Tseng GN. MinK-related peptide 1 associates with Kv4.2 and modulates its gating function: potential role as beta subunit of cardiac transient outward channel? Circ Res 2001;88:1012–1019.
14. Delpon E, Cordeiro JM, Nunez L, et al. Functional effects of KCNE3 mutation and its role in the development of Brugada syndrome. Circ Arrhythm Electrophysiol 2008;1:209–218.
15. Roepke TK, Kontogeorgis A, Ovanez C, et al. Targeted deletion of *KCNE2* impairs ventricular repolarization via disruption of $I_{K,slow1}$ and $I_{to,f}$. FASEB J 2008;22:3648–3660.
16. Calloe K, Cordeiro JM, Di Diego JM, et al. A transient outward potassium current activator recapitulates the electrocardiographic manifestations of Brugada syndrome. Cardiovasc Res 2009;81:686–694.
17. Dixon JE, Shi W, Wang HS, et al. Role of the Kv4.3 K^+ channel in ventricular muscle. A molecular correlate for the transient outward current. Circ Res 1996;79:659–668.
18. Kääb S, Dixon J, Duc J, et al. Molecular basis of transient outward potassium current downregulation in human heart failure: a decrease in Kv4.3 mRNA correlates with a reduction in current density. Circulation 1998;98:1383–1393.
19. Benitah JP, Gomez AM, Bailly P, et al. Heterogeneity of the early outward current in ventricular cells isolated from normal and hypertrophied rat hearts. J Physiol 1993;469:111–138.
20. Singleton CB, Valenzuela SM, Walker BD, et al. Blockade by N-3 polyunsaturated fatty acid of the Kv4.3 current stably expressed in Chinese hamster ovary cells. Br J Pharmacol 1999;127:941–948.
21. Deschênes I, Tomaselli GF. Modulation of Kv4.3 current by accessory subunits. FEBS Lett 2002;528:183–188.
22. Wang S, Bondarenko VE, Qu Y, Morales MJ, Rasmusson RL, Strauss HC. Activation properties of Kv4.3 channels: time, voltage and $[K^+]_o$ dependence. J Physiol 2004;557:705–717.
23. An WF, Bowlby MR, Betty M, et al. Modulation of A-type potassium channels by a family of calcium sensors. Nature 2000;403:553–556.
24. Decher N, Uyguner O, Scherer CR, et al. hKChIP2b is a functional modifier of hKv4.3 potassium channels: cloning and expression of a short hKChIP2b splice variant. Cardiovasc Res 2001;52:255–264.
25. Radicke S, Cotella D, Graf EM, et al. Functional modulation of the transient outward current I_{to} by *KCNE* beta-subunits and regional distribution in human non-failing and failing hearts. Cardiovasc Res 2006;1:695–703.
26. Deschênes I, DiSilvestre D, Juang GJ, Wu RC, An WF, Tomaselli GF. Regulation of Kv4.3 current by KChIP2b splice variants: a component of native cardiac I_{to}? Circulation 2002;106:423–429.
27. Radicke R, Vaquero M, Caballero R, et al. Effects of MiRP1 and DPP6 β-subunits on the blockade induced by flecainide of Kv4.3/KChIP2 channels. Br J Pharmacol 2008;154:774–786.
28. Wettwer E, Amos GJ, Posival H, Ravens U. Transient outward current in human ventricular myocytes of subepicardial and subendocardial origin. Circ Res 1994; 75:473–482.
29. Patel SP, Campbell DL. Transient outward potassium current, "I_{to}," phenotypes in the mammalian left ventricle: underlying molecular, cellular and biophysical mechanisms. J Physiol 2005;569:7–39.
30. Antzelevitch C. Brugada syndrome. Pacing Clin Electrophysiol 2006;29:1130–1159.
31. Bezzina C, Veldkamp MW, van den Berg MP, et al. A single Na^+ channel mutation causing both long-QT and Brugada syndromes. Circ Res 1999;85: 1206–1213.
32. Van den Berg MP, Wilde AA, Viersma TJW, et al. Possible bradycardic mode of death and successful pacemaker treatment in a large family with features of long QT syndrome type 3 and Brugada syndrome. J Cardiovasc Electrophysiol 2001;12:630–636.